Article

Cell

Common *PIEZO1* Allele in African Populations Causes RBC Dehydration and Attenuates *Plasmodium* Infection

Graphical Abstract

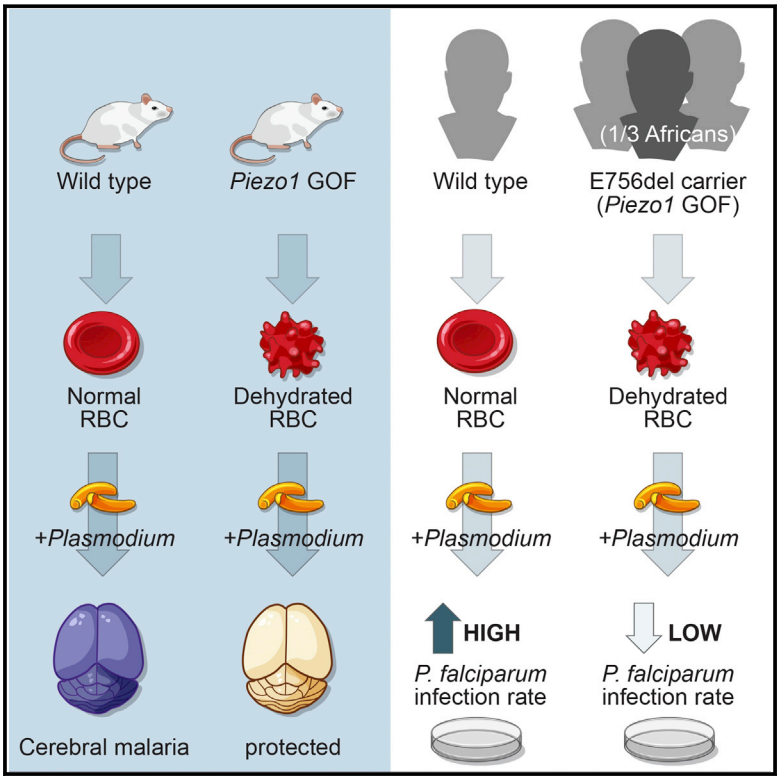

Authors

Shang Ma, Stuart Cahalan, Gregory LaMonte, ..., Elizabeth A. Winzeler, Kristian G. Andersen, Ardem Patapoutian

Correspondence

ardem@scripps.edu

In Brief

A gain-of-function mutation in the mechanically activated channel PIEZO1 is associated with resistance to the malaria parasite *Plasmodium falciparum*.

Highlights

- Expression of a gain-of-function *Piezo1* allele models hereditary xerocytosis in mice
- Mice expressing gain-of-function *Piezo1* allele are protected from cerebral malaria
- A third of the African population carry a *PIEZO1* gain-of-function allele (E756del)
- RBCs from E756del carriers are dehydrated and show reduced susceptibility to *Plasmodium*

Ma et al., 2018, Cell *173*, 443–455
April 5, 2018
https://doi.org/10.1016/j.cell.2018.02.047

CellPress

Article

Cell

Common *PIEZO1* Allele in African Populations Causes RBC Dehydration and Attenuates *Plasmodium* Infection

Shang Ma,[1] Stuart Cahalan,[1,10] Gregory LaMonte,[2] Nathan D. Grubaugh,[3] Weizheng Zeng,[1] Swetha E. Murthy,[1] Emma Paytas,[2] Ramya Gamini,[4] Viktor Lukacs,[1] Tess Whitwam,[1] Meaghan Loud,[1] Rakhee Lohia,[5] Laurence Berry,[5] Shahid M. Khan,[6] Chris J. Janse,[6] Michael Bandell,[7] Christian Schmedt,[7] Kai Wengelnik,[5] Andrew I. Su,[4] Eric Honore,[8,9] Elizabeth A. Winzeler,[2] Kristian G. Andersen,[3,4] and Ardem Patapoutian[1,11,*]

[1]Howard Hughes Medical Institute, Department of Neuroscience, Dorris Neuroscience Center, The Scripps Research Institute, La Jolla, CA 92037, USA

[2]Division of Host-Microbe Systems & Therapeutics, Department of Pediatrics, University of California, San Diego, San Diego, CA, USA

[3]Department of Immunology and Microbiology, The Scripps Research Institute, La Jolla, CA, USA

[4]Department of Integrative, Structural and Computational Biology, The Scripps Research Institute, La Jolla, CA, USA

[5]DIMNP, CNRS, INSERM, University Montpellier, Montpellier, France

[6]Leiden Malaria Research Group, Department of Parasitology, Leiden University Medical Center (LUMC), 2333ZA Leiden, the Netherlands

[7]Genomics Institute of the Novartis Research Foundation, La Jolla, CA, USA

[8]Université Côte d'Azur, Centre National de la Recherche Scientifique, Paris, France

[9]Institut de Pharmacologie Moléculaire et Cellulaire, Labex ICST, Valbonne, France

[10]Present address: Vertex Pharmaceuticals, 11010 Torreyana Road, San Diego, CA 92121, USA

[11]Lead Contact

*Correspondence: ardem@scripps.edu

https://doi.org/10.1016/j.cell.2018.02.047

SUMMARY

Hereditary xerocytosis is thought to be a rare genetic condition characterized by red blood cell (RBC) dehydration with mild hemolysis. RBC dehydration is linked to reduced *Plasmodium* infection *in vitro*; however, the role of RBC dehydration in protection against malaria *in vivo* is unknown. Most cases of hereditary xerocytosis are associated with gain-of-function mutations in PIEZO1, a mechanically activated ion channel. We engineered a mouse model of hereditary xerocytosis and show that *Plasmodium* infection fails to cause experimental cerebral malaria in these mice due to the action of Piezo1 in RBCs and in T cells. Remarkably, we identified a novel human gain-of-function *PIEZO1* allele, E756del, present in a third of the African population. RBCs from individuals carrying this allele are dehydrated and display reduced *Plasmodium* infection *in vitro*. The existence of a gain-of-function PIEZO1 at such high frequencies is surprising and suggests an association with malaria resistance.

INTRODUCTION

PIEZOs are non-selective cation channels that sense mechanical stimuli in many multicellular organisms (Coste et al., 2010; Ranade et al., 2015). PIEZO1 is essential for mechanotransduction in vascular development, blood pressure regulation, and red blood cell (RBC) volume control, among other roles (Li et al., 2014; Ranade et al., 2014b; Retailleau et al., 2015; Wang et al., 2016; Cahalan et al., 2015). The related PIEZO2 is the principal mechanosensor for touch and proprioception (Ranade et al., 2014a; Woo et al., 2014, 2015; Chesler et al., 2016). Human genetic studies have highlighted the significance of PIEZO1 in human development and physiology. Patients with loss-of-function mutations in *PIEZO1* suffer from persistent lymphedema caused by congenital lymphatic dysplasia (Lukacs et al., 2015). *PIEZO1* mutations are also linked to hereditary xerocytosis, also known as dehydrated hereditary stomatocytosis (Zarychanski et al., 2012; Albuisson et al., 2013; Bae et al., 2013). Hereditary xerocytosis is a dominantly inherited blood disorder characterized by RBC dehydration causing reduced RBC osmotic fragility and is associated with mild or asymptomatic hemolysis (Delaunay, 2004). This disorder is considered to be rare and found mostly in the Caucasian population (Archer et al., 2014; Glogowska et al., 2017). Complications include splenomegaly, resulting from increased RBC trapping in the spleen, as well as iron overload due to unknown mechanisms (Archer et al., 2014). 19 different point mutations in PIEZO1 have been described to cause hereditary xerocytosis (Murthy et al., 2017). Some of these mutations have been electrophysiologically analyzed and show slower inactivation kinetics compared to wild-type PIEZO1 channels. The slower inactivation translates to more ions passing through PIEZO ion channels, and thus these mutations are considered gain of function. Consistently, *Piezo1* deficiency in RBCs in mice causes overhydration (Cahalan et al., 2015). Beyond RBCs, studies in mice have suggested wide-ranging functions of PIEZO1 in various biological processes; whether hereditary xerocytosis is associated with other conditions beyond RBC pathology is currently not fully understood.

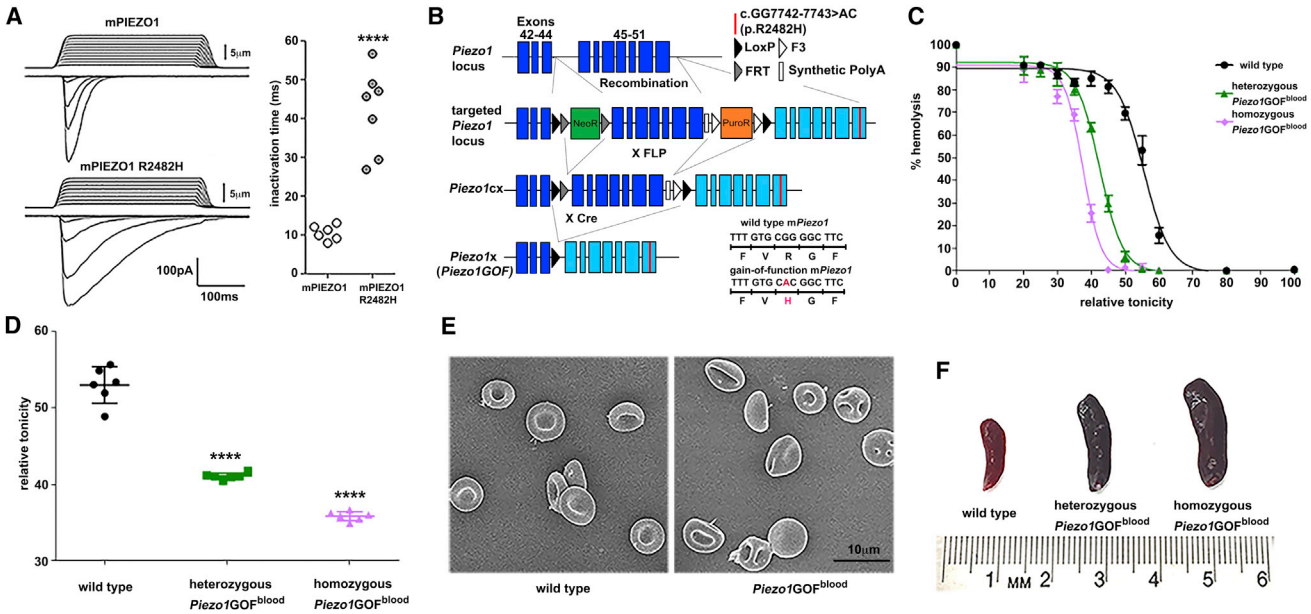

Figure 1. Mouse Model for Human Xerocytosis

(A) Representative traces of mechanically activated (MA) inward currents for wild-type and mPIEZO1 R2482H. ****$p < 0.001$.

(B) Strategy for generating knockin mouse.

(C) Osmotic fragility test for RBCs.

(D) Quantification for osmotic fragility. Relative tonicity at which 50% RBCs are lysed (half hemolysis) was calculated for each curve. ****$p < 0.001$.

(E) Scanning electron microcopy images. Heterozygous *Piezo1*GOF ^{blood} RBCs showed signs of stomatocytes.

(F) Splenomegaly in gain-of-function *Piezo1* mice (Figure S1C).

Scale bar, 10 μm. Data are presented as means ± SEM. See also Figure S1 and Table S1.

Plasmodium, the causative parasite for malaria, has exerted strong selective pressures on the human genome (Kwiatkowski, 2005). This is demonstrated by severe genetic conditions, such as sickle cell disease, that persist in human populations from malaria-endemic areas because the underlying genetic variants confer resistance to *Plasmodium* infection (Hedrick, 2004; Feng et al., 2004). The scope of RBC disorders that might contribute to *Plasmodium* resistance, however, has not been fully explored. Interestingly, dehydrated RBCs (including those from hereditary xerocytosis patients) show delayed infection rates to *Plasmodium in vitro*, suggesting a potential protective mechanism against infections from this parasite (Tiffert et al., 2005). The effects of dehydrated RBC on *Plasmodium* infection *in vivo*, however, remain unknown. Since overactive PIEZO1 causes dehydrated RBCs in hereditary xerocytosis patients, we reasoned that mice carrying a gain-of-function *Piezo1* allele could offer a suitable model to investigate the effect of *Plasmodium* infection *in vivo* (de Oca et al., 2013).

RESULTS

Piezo1 Gain-of-Function Mice Recapitulate Human Hereditary Xerocytosis Phenotypes

To test whether gain-of-function *Piezo1* expression causes xerocytosis-like phenotypes in mice, and to elucidate the role of xerocytosis in *Plasmodium* infection *in vivo*, we engineered mice that conditionally express a human-equivalent hereditary xerocytosis mutation (Figure 1). Specifically, R2456H is a xerocytosis mutation in human *PIEZO1* that displays significantly longer channel inactivation time (τ) (Albuisson et al., 2013). We verified that the equivalent mouse *Piezo1* point mutation (R2482H), when overexpressed in HEK cells that lack endogenous *PIEZO1* (*PIEZO1*KO HEK) (Dubin et al., 2017), showed slower channel inactivation (Figure 1A). Since residue 2482 resides in the last coding exon (51), we designed the knockin construct by flanking exons 45–51 with *loxP* sites, followed by a copy of the region containing exons 45–51 with a mutation that would replace R with H at residue 2482 (Figure 1B). We named this conditional allele *Piezo1*^{cx}. In cells that express Cre recombinase, the wild-type exon will be replaced by the modified exon, allowing tissue-specific control of gain-of-function *Piezo1* expression.

We generated a constitutive gain-of-function *Piezo1* mouse line by crossing mice homozygous for the mutant allele (*Piezo1*$^{cx/cx}$) with cmv-cre mice that expressed a Cre driver ubiquitously (Schwenk et al., 1995). We also generated a hematopoietic lineage-specific gain-of-function *Piezo1* mouse line (*Piezo1*GOF ^{blood}) using vav1-cre (de Boer et al., 2003). To evaluate the expression of the gain-of-function allele, we sequenced the last exon of *Piezo1* cDNA from whole blood of homozygous *Piezo1*GOF ^{blood} and observed the expected nucleotide change c.GG$_{7742\text{-}7743}$AC (Figure S1A). In addition, we found that *Piezo1* transcript levels in whole blood from both homozygous and heterozygous *Piezo1*GOF ^{blood} mice were similar to levels observed in wild-type mice, demonstrating that the genetic manipulation did not

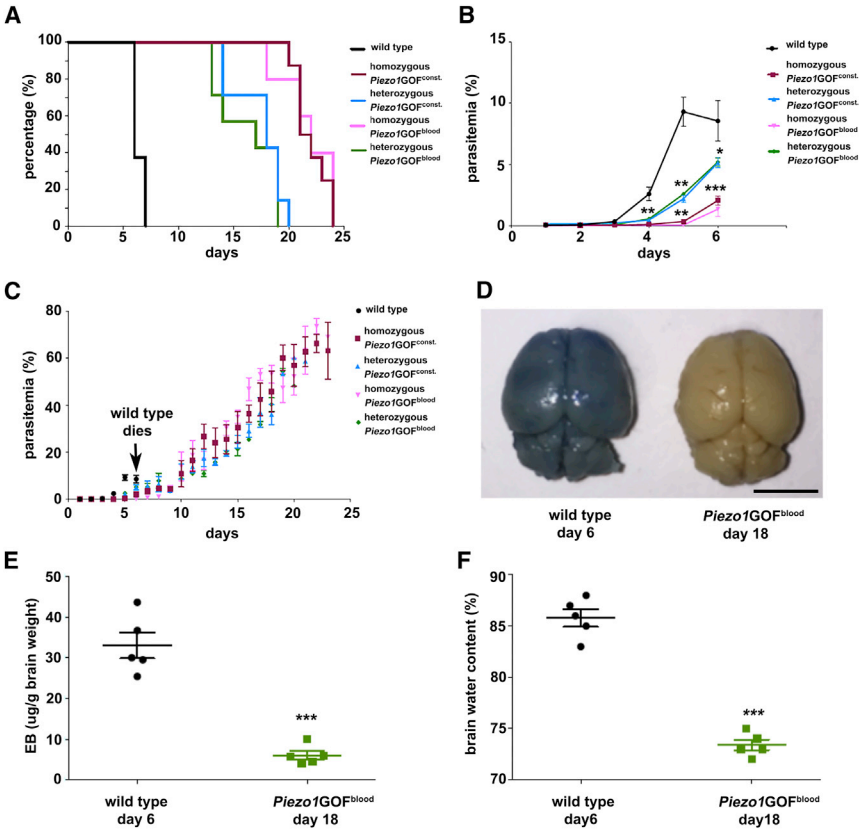

Figure 2. *Plasmodium* Infection in Gain-of-Function *Piezo1* Mice

(A) Survival curves for gain-of-function *Piezo1* mice after *P. berghei* infected RBCs.

(B and C) Parasitemia recorded by flow cytometry for phase 1 (first 7 days, B) and phase 1 and 2 together (24 days, C), respectively.

(D) Intact blood-brain barrier in infected gain-of-function *Piezo1* mice.

(E) Quantification of blood-brain barrier disruption.

(F) Brain water content in infected brains.

*p < 0.05, **p < 0.01, and ***p < 0.001. Scale bar, 5 mm. Data are presented as means ± SEM.

alter *Piezo1* expression levels (Figure S1B). We also found that both constitutive (*Piezo1*GOF ^{constitutive}) and blood-cell-specific (*Piezo1*GOF ^{blood}) transgenic mice (heterozygous and homozygous) were born at the expected Mendelian ratio and appeared to develop normally.

We found that RBCs from both homozygous and heterozygous *Piezo1*GOF ^{blood} mice showed reduced osmotic fragility, as shown by a left-shifted curve in a hypotonicity-dependent hemolysis challenge (Figures 1C and 1D). This demonstrates that RBCs from gain-of-function *Piezo1* mice are more resistant to lysis in response to hypotonic solutions compared to wild-type, a defining feature for hereditary xerocytosis (Archer et al., 2014). *Piezo1*GOF ^{blood} mice also displayed hematological properties similar to mild anemia, indicated by a lower hemoglobin level and increased reticulocyte number, as is the case for individuals with hereditary xerocytosis (Table S1). Those patients also have increased mean corpuscular volume, which is a measure of RBC volume, and increased mean corpuscular hemoglobin, which indicates average hemoglobin mass per RBC (Zarychanski et al., 2012; Albuisson et al., 2013; Bae et al., 2013; Archer et al., 2014). We found that shifts in these two values in gain-of-function *Piezo1* mice were similar to those observed in hereditary xerocytosis patients. Mean cell hemoglobin concentration, in contrast—which is expected to be elevated in dehydrated RBCs—was not significantly increased in homozygous *Piezo1*GOF ^{blood} mice. Importantly, however, we found that RBCs from these mice were nevertheless dehydrated, as they showed reduced osmotic fragility (Figures 1C and 1D). In addition, we used scanning electron microscopy and found the presence of RBCs with deformed and dehydrated shapes from heterozygous *Piezo1*GOF ^{blood} mice, which is another clinical feature often observed in patients (Figure 1E). One of the predominant features of hereditary xerocytosis is splenomegaly. We found that both homozygous and heterozygous *Piezo1*GOF ^{blood} mice had significantly larger spleens (1.04 ± 0.03, 0.74 ± 0.02 cm^2, respectively) compared to wild-types (0.42 ± 0.02 cm^2, n = 4 animals per genotype, Student's t test, compared to wild-type, $p < 1 \times 10^{-4}$) (Figures 1F and S1C). Together, our data show that gain-of-function *Piezo1* mice display hallmark clinical features observed in human hereditary xerocytosis patients, including RBC dehydration, mild anemia, and splenomegaly.

Gain-of-Function *Piezo1* Mice Have Reduced Growth Rate of *Plasmodium* Blood Stages and Protect against Experimental Cerebral Malaria

To evaluate the connection between Piezo1, RBC dehydration, and protection against malaria, we infected gain-of-function Piezo1 mice with a GFP-expressing reference line of the ANKA strain of rodent malaria parasite *Plasmodium berghei* (Franke-Fayard et al., 2004). We chose *P. berghei* ANKA since this parasite is a well-established model to analyze the course of infections *in vivo*, and to investigate experimental cerebral malaria in mice (Franke-Fayard et al., 2004; de Souza et al., 2010; Hunt et al., 2010). We found that wild-type mice died between day 6 and 8, consistent with previous findings (Franke-Fayard et al., 2004; de Oca et al., 2013) (Figure 2A). In contrast, we observed that the homozygous and heterozygous *Piezo1*GOF ^{constitutive} mice survived as long as 24 and 19 days, respectively (Figure 2A). Importantly, the post-infection survival rates of *Piezo1*GOF ^{blood} mice were indistinguishable from *Piezo1*GOF ^{constitutive} mice, indicating that induction of gain-of-function *Piezo1* in hematopoietic lineages was sufficient to extend post-infection survival (Figure 2A).

Next, we analyzed the course of infection in wild-type and gain-of-function *Piezo1* mice to test whether the expression of

the mutant Piezo1 allele affects *Plasmodium* growth rate in RBCs, as suggested by previous *in vitro* experiments (Tiffert et al., 2005). We measured the percentage of RBCs that were GFP positive (parasitemia) by flow cytometry. During the first week of infection (phase 1, Figure 2B), we found that parasitemia reached 6%–12% in wild-type mice at the time of death; however, both *Piezo1*GOF ^{constitutive} and *Piezo1*GOF ^{blood} mice had significantly lower parasitemia (on day 6, 5.14% ± 0.42% for constitutive mice and 5.20% ± 0.34% for blood-cell-specific mice, $p < 0.05$ compared to wild-type, 8.53% ± 1.65%, Student's t test). These findings suggest that expression of a gain-of-function *Piezo1* allele in blood cells reduce parasite growth rate of blood stages (Figure 2B). Unlike wild-type animals, which all died at the end of phase 1, gain-of-function *Piezo1* mice then entered a second phase of infection (phase 2; day 7 to day 23, Figure 2C). We found that during this phase, they exhibited a steady increase in parasitemia, eventually leading to severe hyperparasitemia of up to 70% of infected RBCs (Figures 2B and 2C). These data suggest that gain-of-function *Piezo1* expression can dramatically modify the course of *Plasmodium* infection *in vivo*, leading to enhanced survival, despite high end-stage levels of parasitemia (Figure 2C).

A prominent feature of experimental cerebral malaria in the *P. berghei* ANKA/C57BL/6 infection model is the breakdown of blood-brain barrier (Nacer et al., 2014). We injected Evans blue dye into mice and studied blood-brain barrier compromise. As expected, we observed blue dye leakage into brain parenchyma in all wild-type mice at day 6 after infection (n = 8) (Figure 2D, left), indicating blood-brain barrier breakdown. Remarkably, we did not detect Evans blue leakage in the brains of *Piezo1*GOF ^{blood} (n = 7) even at day 18 when they were about to die (Figure 2D, right). To quantitatively evaluate blood-brain barrier disruption, we measured the optical density of Evans blue dyes extracted from infected brains (n = 5 per genotype) (Ferreira et al., 2011). We observed a significant reduction in brain Evans blue contents in infected *Piezo1*GOF ^{blood} compared to wild-type mice (Figure 2E). In addition, we evaluated experimental cerebral malaria by measuring brain water content that reflects the severity of brain edema caused by cerebral complications (Hunt et al., 2014). Wild-type mice had increased brain water content after infection compared to *Piezo1*GOF ^{blood} mice (Figure 2F). Thus, our data show that gain-of-function *Piezo1*-expressing mice are protected against experimental cerebral malaria. However, these mice eventually died, probably due to severe anemia, as they showed reduced hemoglobin (HGB) levels (2.85 ± 2.5 g/dL, n = 3, in *Piezo1*GOF ^{blood} mice 18 days after infection) compared to uninfected *Piezo1*GOF ^{blood} mice (14.02 ± 0.16 g/dL, n = 5, $p < 0.002$) (Phillips and Pasvol, 1992). Together, our results suggest that gain-of-function *Piezo1* expression reduces *Plasmodium* growth rate of blood-stage infection *in vivo* and can protect mice from the development of cerebral complications. The reduced *Plasmodium* infection rate of dehydrated RBCs observed *in vitro* (Tiffert et al., 2005) can explain the reduced parasite growth rate of blood stage observed in gain-of-function *Piezo1* mice during phase 1; however, a connection between dehydrated RBCs and protection from experimental cerebral malaria was novel and unexpected.

RBC Dehydration Is Responsible for Reduced Parasite Growth and Partially Responsible for Protection against Cerebral Malaria in Gain-of-Function *Piezo1* Mice

To address whether decreased parasite growth rate and prevention of experimental cerebral malaria in the gain-of-function *Piezo1* mice were due to RBC dehydration, we genetically rescued RBC dehydration in gain-of-function *Piezo1* mice and assessed *P. berghei* infection. We took advantage of the fact that PIEZO1-induced RBC dehydration requires the activity of KCa3.1, a calcium-dependent potassium channel (also known as Gardos channel). Activation of KCa3.1 drives potassium and water out of RBCs in response to increased intracellular calcium, thereby causing dehydration (Maher and Kuchel, 2003; Cahalan et al., 2015). We crossed the gain-of-function *Piezo1* mice to *KCa3.1* knockout mice. As expected, *Piezo1*GOF ^{blood}/*KCa3.1*$^{-/-}$ mice had osmotic fragility similar to wild-type mice, demonstrating that RBC dehydration was corrected by removing KCa3.1 channel activity (Figures 3A and S2). After *P. berghei* ANKA infection, *Piezo1*GOF ^{blood}/*KCa3.1*$^{-/-}$ mice survived significantly longer than wild-type (but shorter than *Piezo1*GOF ^{blood}). This resulted in an intermediate survival curve of *Piezo1*GOF ^{blood}/*KCa3.1*$^{-/-}$ mice ($p < 0.0001$, compared to wild-type and *Piezo1*GOF ^{blood}) (Figure 3B). This suggests that correction of RBC dehydration fails to reverse survival rate to a level that is similar to wild-type, indicating that RBC dehydration is not completely responsible for the increased survival rate in the gain-of-function *Piezo1* mice.

We also found that *Piezo1*GOF ^{blood}/*KCa3.1*$^{-/-}$ mice had a parasite growth rate of blood stage that was indistinguishable from that of wild-type during the first week of infection, suggesting that RBC dehydration was responsible for the reduced parasite growth observed during phase 1 in gain-of-function *Piezo1* mice (Figure 3C). Importantly, *KCa3.1* knockout mice in wild-type *Piezo1* background did not show changes in parasitemia, suggesting that the absence of *KCa3.1 per se* did not influence RBC infection (Figure 3C, gray). Finally, quantitative measurements of both Evans blue and brain water content in infected brains showed that *Piezo1*GOF ^{blood}/*KCa3.1*$^{-/-}$ mice experienced an intermediate level of cerebral complications between wild-type and *Piezo1*GOF ^{blood} mice (Figures 3D–3F). Together, our data from *Piezo1*GOF ^{blood}/*KCa3.1*$^{-/-}$ genetic experiments suggest that (1) RBC dehydration is completely responsible for the reduced parasite growth rate (phase 1); and (2) RBC dehydration is a major contributing factor for the absence of experimental cerebral malaria (phase 2), but that other mechanisms may be involved.

Gain-of-Function *Piezo1* Expression in RBCs and T Cells Contributes to Protection against Cerebral Malaria

The incomplete protection from experimental cerebral malaria in *Piezo1*GOF ^{blood}/*KCa3.1*$^{-/-}$ mice (despite normal parasite growth rate) suggests the existence of other mechanisms that affect cerebral complication in gain-of-function *Piezo1* mice. Previous work has shown that processes critical for the development of cerebral malaria in both humans and rodents involve both RBCs and immune cells (Baptista et al., 2010; Nacer et al., 2014; Dunst et al., 2017). To directly address the cell autonomous function of gain-of-function *Piezo1* allele in these cells, we induced expression of gain-of-function *Piezo1* mutation

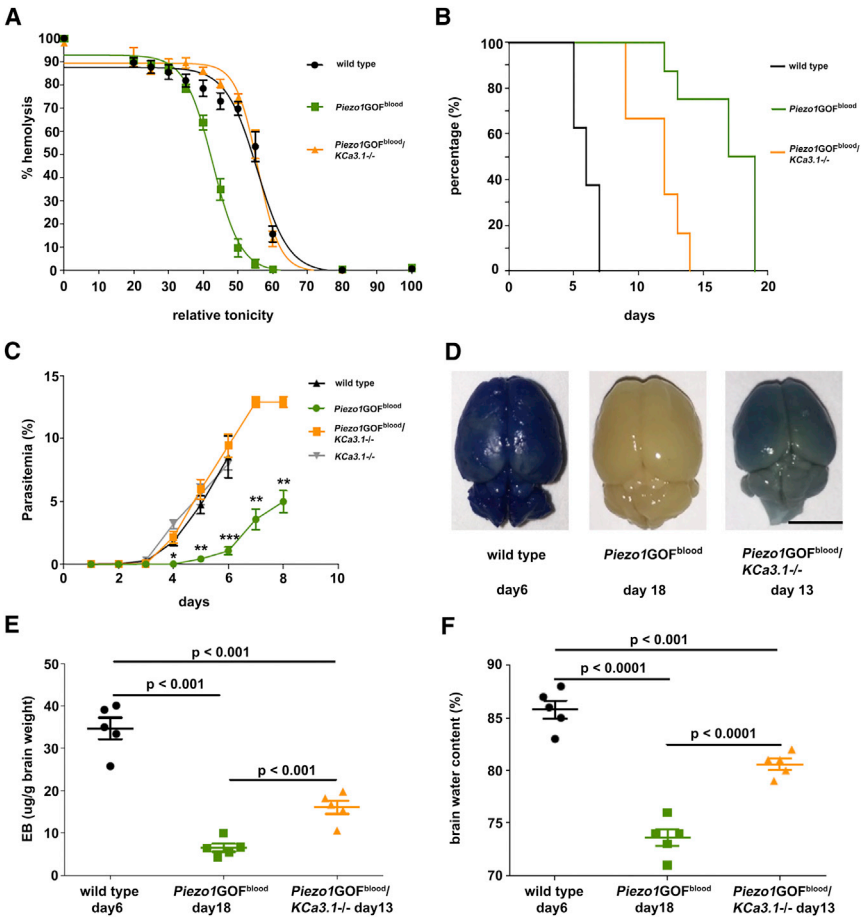

Figure 3. Role of RBC Dehydration in *Plasmodium* Infection in Mice

(A) Deletion of *KCa3.1* in heterozygous *Piezo1*GOF ^{blood} mice (orange) restored RBC dehydration in heterozygous *Piezo1*GOF ^{blood} (green). *Piezo1*GOF ^{blood}/*KCa3.1*$^{-/-}$ mice had a similar curve to wild-type.

(B) Post infection survival rate of *Piezo1*GOF ^{blood}/*KCa3.1*$^{-/-}$ mice (orange) is intermediate between wild-type (black) and heterozygous *Piezo1*GOF ^{blood} mice (green). $p < 0.0001$, Mantel-Cox tests.

(C) Both *Piezo1*GOF ^{blood}/*KCa3.1*$^{-/-}$ and *KCa3.1*$^{-/-}$ mice had same parasitemia as wild-type, with significantly higher than heterozygous *Piezo1*GOF ^{blood} mice.

(D) Breakdown of blood-brain barrier in *Piezo1*GOF ^{blood}/*KCa3.1*$^{-/-}$ mice 13 days after infection.

(E) Quantification for blood-brain barrier disruption.

(F) Brain water content in infected brains.

*$p < 0.05$, **$p < 0.01$, and ***$p < 0.001$. Scale bar, 5 mm. Data are presented as means ± SEM. See also Figure S2.

in different blood cell types and tested survival rate, parasite growth rate, and experimental cerebral malaria.

First, we generated RBC-specific gain-of-function *Piezo1* mice (*Piezo1*GOF ^{RBC}) with EpoR-cre (Heinrich et al., 2004). We verified the efficiency and specificity of EpoR-cre expression by measuring RBC osmotic fragility for *Piezo1*GOF ^{RBC} mice. We found that these mice had reduced RBC fragility, similar to *Piezo1*GOF ^{blood} mice, suggesting that EpoR-cre was efficiently inducing recombinase activity in most RBCs (Figures 4A and S3A). Also, gain-of-function *Piezo1* mRNA was not present in immune cells (CD4$^+$ and CD8$^+$ T cells) from *Piezo1*GOF ^{RBC} mice. This is an important control, as we address the role of gain-of-function *Piezo1* expression in T cells separately (see below) (Figure S4B). We found that infection of *Piezo1*GOF ^{RBC} mice with *P. berghei* caused a survival rate indistinguishable from *Piezo1*GOF ^{blood} mice (Figure 4B). Furthermore, *Piezo1*GOF ^{RBC} mice had a parasitemia curve indistinguishable from *Piezo1*GOF ^{blood} mice and did not develop experimental cerebral malaria (Figures 4C and 4D). These data suggest that the expression of gain-of-function *Piezo1* in RBCs is sufficient to cause reduced *Plasmodium* growth rates and to protect mice from the development of cerebral complications.

Parasite-specific CD8$^+$ cells are essential in causing *Plasmodium*-induced cerebral complications (Yañez et al., 1996; Belnoue et al., 2002; Howland et al., 2015). We induced gain-of-function *Piezo1* expression in peripheral CD4$^+$ and CD8$^+$ T cells by using hCD2-cre (Vacchio et al., 2014). We tested the specificity of hCD2-cre by measuring RBC osmotic fragility and showed that *Piezo1*$^{cx/+}$; hCD2-cre (*Piezo1*GOF $^{T\ cells}$) mice had normal RBC fragility, confirming that hCD2-cre did not induce gain-of-function *Piezo1* expression in RBCs (Figures 4A and S3A). Furthermore, we evaluated the efficiency of hCD2-cre in targeting CD4$^+$ and CD8$^+$ T cells by sequencing the cDNA made by those cells from homozygous *Piezo1*GOF $^{T\ cells}$ mice and found that gain-of-function *Piezo1* mRNA was the only *Piezo1* transcript expressed in the targeted cells (Figure S3B).

We found that, after *P. berghei* infection, *Piezo1*GOF $^{T\ cells}$ mice survived significantly longer than wild-type mice ($p < 0.01$), but not as long as *Piezo1*GOF ^{blood} or *Piezo1*GOF ^{RBC} mice ($p < 0.01$), suggesting that expression of gain-of-function *Piezo1* in T cells provided partial protection (Figure 4B). Furthermore, we found that parasitemia in *Piezo1*GOF $^{T\ cells}$ mice was identical to that of wild-type mice during the first 7 days after infection, before it continued climbing until the end of the infection (Figure 4C, compare dark blue and black). This suggested that gain-of-function *Piezo1* expression in CD4/8$^+$ T cells did not alter parasite growth rate of blood stage compared to wild-type mice (phase 1). Intriguingly, despite wild-type-like parasite growth rates during the first 7 days, *Piezo1*GOF $^{T\ cells}$ mice displayed attenuated experimental cerebral malaria during phase 2 (Figures 4D and 4E). Also, *Piezo1*GOF $^{T\ cells}$ mice had an intermediate level of cerebral complications between wild-type and *Piezo1*GOF ^{RBC} mice (Figure 4F). These data demonstrate that gain-of-function *Piezo1* expression in T cells can provide partial survival advantage by attenuating the disruption of the blood-brain barrier seen in experimental cerebral malaria.

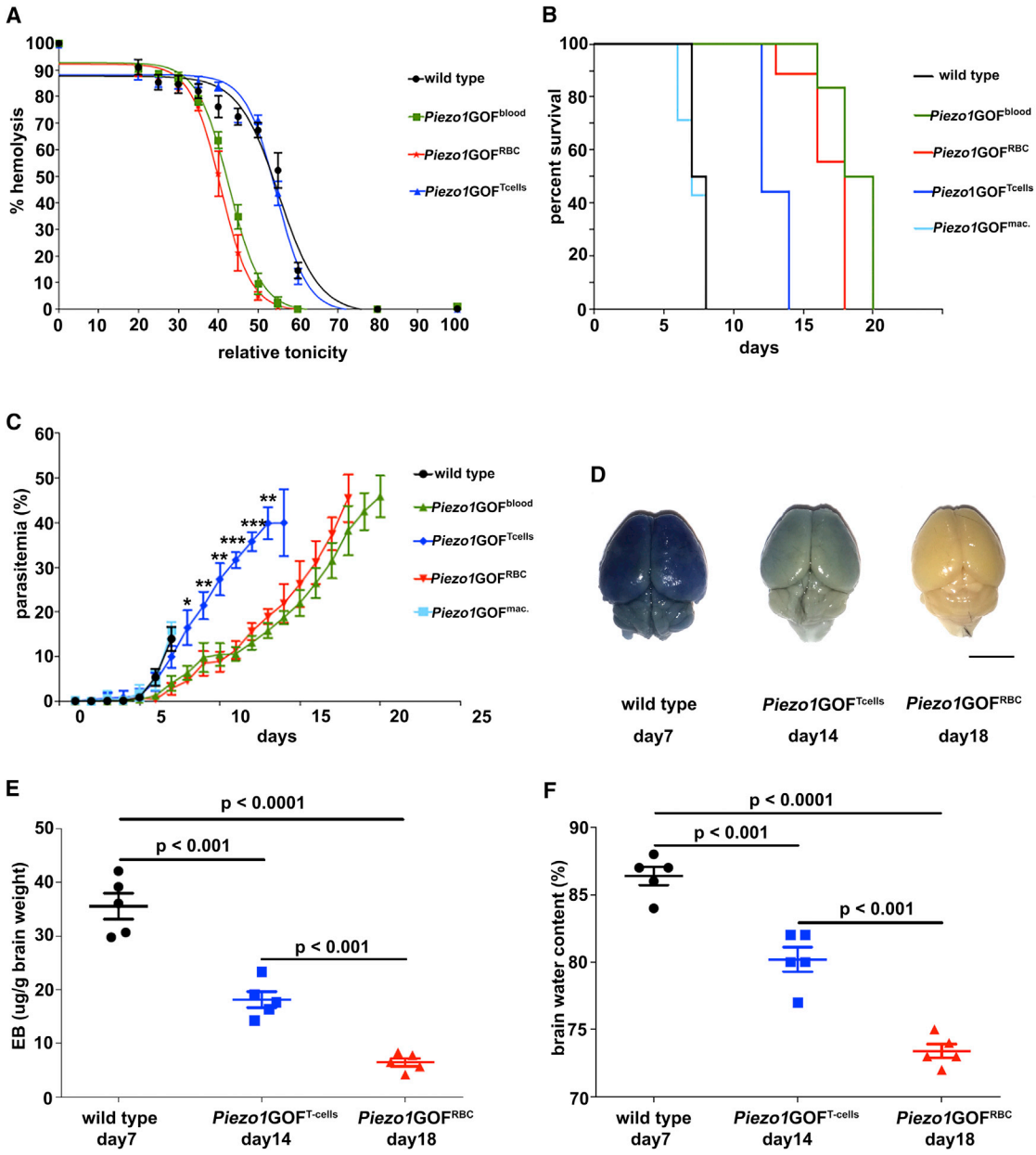

Figure 4. Role of Gain-of-Function *Piezo1* Expression in RBCs and T Cells during *Plasmodium* Infection in Mice

(A) RBC osmotic fragility for different gain-of-function *Piezo1* mice.

(B) Mice with gain-of-function *Piezo1* in different blood cells had distinct survival rates after infection. *Piezo1*GOF ^{RBC} (red) had survival rate similar to pan-blood-cell-specific mice (*Piezo1*GOF ^{blood} [green]), $p > 0.05$. Macrophage-specific gain-of-function mice (*Piezo1*GOF ^{macrophage}) had same survival rate as wild-type, $p > 0.05$. *Piezo1*GOF $^{T\ cells}$ had a survival rate greater than wild-type ($p < 0.01$) and less than *Piezo1*GOF ^{blood} mice ($p < 0.01$). Mantel-Cox tests.

(C) Parasitemia recorded by flow-cytometry for gain-of-function mice. *$p < 0.05$, **$p < 0.01$, and ***$p < 0.001$, Student's t test.

(D) Blood-brain barrier compromise in T cell- and RBC-specific gain-of-function mice after infection.

(E) Quantification for blood-brain barrier disruption.

(F) Brain water content in infected brains.

Scale bar, 5 mm. Data are presented as means ± SEM. See also Figure S3.

Finally, we tested whether gain-of-function *Piezo1* expression in macrophages can affect *Plasmodium* infection, since macrophages have been shown to be important for both protection and pathology in malaria (Chua et al., 2013). We expressed gain-of-function *Piezo1* specifically in macrophages using LysM-cre (Clausen et al., 1999). *Piezo1*GOF ^{macrophage} mice displayed survival rate (Figure 4B) and parasitemia curves similar to wild-type littermates (Figure 4C). These results indicate that

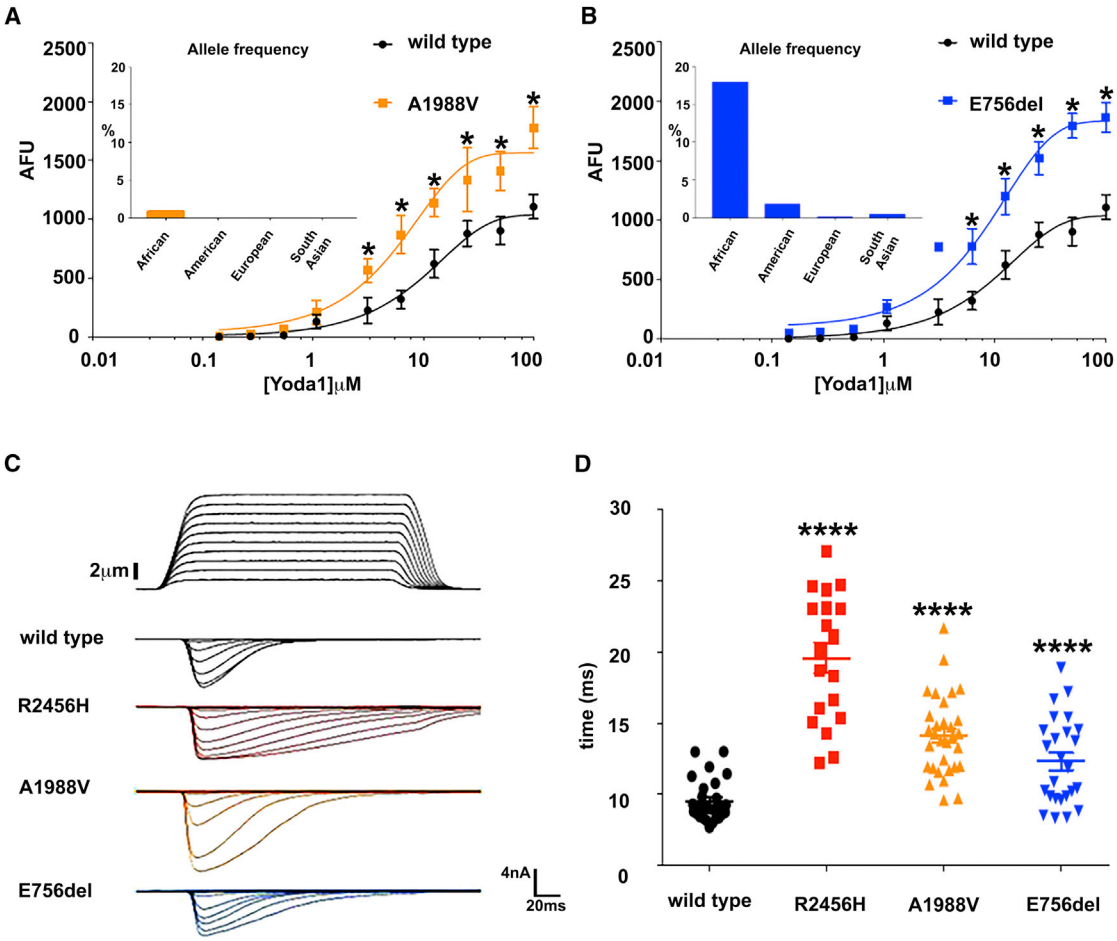

Figure 5. Identification of Gain-of-Function *PIEZO1* Mutations in African Populations

(A and B) Yoda1-induced intracellular calcium signals in *PIEZO1*KO HEK cells overexpressing A1988V (A) and E756del (B) cDNA (*$p < 0.05$). Allele frequency for both mutations is shown in the insets.

(C) Representative traces of mechanically activated (MA) inward currents for wild-type and mutated cDNA. R2456H, A1988V, and E756del mutations.

(D) Quantification for inactivation time (τ).

each point = a single cell. ***$p < 0.001$, **$p < 0.01$. Data are presented as means ± SEM. See also Table S2.

macrophages are unlikely to play an essential role in reducing parasite growth rate and protection against experimental cerebral malaria in xerocytosis mice. Together, our data suggest that RBCs play a major role in gain-of-function *Piezo1*-mediated protection against *Plasmodium* infection and cerebral malaria; however, T cells also appear to be involved in protection against cerebral complications.

Identification of a Common Human *PIEZO1* Gain-of-Function Mutation in African Populations under Positive Selection

The role of gain-of-function PIEZO1 in rodent malaria described here raises a conundrum: if PIEZO1 mutations are protective against *Plasmodium* infection, why then is hereditary xerocytosis not commonly observed in individuals from Africa, where malaria is highly prevalent? To investigate whether common *PIEZO1* gain-of-function mutations are present in African populations, we took a comparative genomics approach to look for possible *PIEZO1* gain-of-function alleles and cataloged nonsynonymous (missense) SNPs and in-frame insertions/deletions (indels) in *PIEZO1*. To maximize the likelihood of finding gain-of-function mutations, we (1) performed our search using the Exome Aggregation Consortium data (ExAC) (Lek et al., 2016); (2) picked *PIEZO1* SNPs or indels with allele frequencies above 0.5%; and (3) picked mutations that were more than 5-fold enriched in African populations, as compared to people of non-African descent. Using these criteria, we found 21 mutations consisting of 19 SNPs and 2 indels (Table S2).

To test for potential functional effects of the various mutations, we next performed a large-scale calcium-imaging assay by screening the 21 candidate mutations for increased response to various concentrations of the PIEZO1 agonist Yoda1 (Syeda et al., 2015). We found that two of the 21 mutations lead to increased PIEZO1 responses in this screen: amino acid substitution A1988V (SNP) and indel E756del (3 nucleotide deletion) (Figures 5A and 5B). We found that the A1988V mutation only has an

allelic frequency of 0.8% in the African population (inset in Figure 5A). In contrast, the E756del mutation has an allelic frequency of 18% in individuals of African descent (3% in Europeans), and therefore present in at least 1 copy in about a third of African population (inset in Figure 5B).

To test whether these mutations lead to gain-of-function PIEZO1 channel kinetics, we recorded mechanically activated currents and found that PIEZO1 variants containing A1988V or E756del mutations was activated normally by mechanical force but had significantly longer inactivation time constants (τ) compared to wild-type ($p < 0.0001$). This is similar to R2456H, a gain-of-function allele that has the longest inactivation time among all hereditary xerocytosis mutations (Albuisson et al., 2013) (Figures 5C and 5D), and the equivalent of this allele was used to create our gain-of-function *Piezo1* mice (Figure 1). These data show that gain-of-function *PIEZO1* mutations with similar ion channel activities to those causing hereditary xerocytosis in Caucasian families (Albuisson et al., 2013) can be found in individuals of African descent. At least one of these, E756del, is present in one-third of African individuals, suggesting a potential connection between PIEZO1, hereditary xerocytosis, and malaria.

We focused on the more abundant allele, E756del. We hypothesized that this allele may be under positive selection in African populations, where malaria is endemic. To test this hypothesis, we assessed three main signatures of selection, commonly found in allelic variants under positive selection (Sabeti et al., 2006): (1) population differentiation of the allele observed between African and non-African populations, as measured by *F*st; (2) whether a variant is in linkage-disequilibrium with nearby SNPs creating a long-range haplotype block, which is commonly observed in more recent (<25,000 years) selective sweeps; and (3) whether the allele is derived (i.e., non-ancestral), since such new alleles typically have low population frequencies, unless under selection.

We looked at the frequency of the E756del allele in the populations present in the 1000 Genomes catalog (Auton et al., 2015) and found that it is present at high allelic frequency (9%–23%) in all populations of African descent, including African Americans (allelic frequency 14%), but not in individuals of non-African ancestry (allelic frequency <1%, Figure 6A). The observed genotype frequencies at this locus are in Hardy-Weinberg equilibrium ($\chi^2 = 0.201$, $p = 0.654$), and therefore segregating as expected in a randomly mating population. Next, we investigated population differentiation across the 1000 Genomes populations. We calculated F_{ST} values at all *PIEZO1* missense mutation loci between individuals of African and non-African descent and found that the populations were most differentiated using the E756del allele (F_{ST} for E756del = 0.32, F_{ST} of all other *PIEZO1* missense alleles = 0–0.26, Figure 6B). This finding is consistent with E756del being under positive selection in populations where malaria is endemic.

We next investigated the regions surrounding the E756del locus but did not observe any SNPs in significant linkage disequilibrium with E756del. The lack of an observed long haplotype flanking this allele makes it harder to conclusively provide proof of positive selection of the E756del variant (Vitti et al., 2013). The lack of linkage disequilibrium, however, could also be because this allele might have been subject to selection on standing variation (i.e., not as the result of a selective sweep [Sabeti et al., 2006]), or because the selective pressure on this locus is relatively old (>25,000 years). Even though *Plasmodium* is an ancient parasite (Loy et al., 2017), the former is still a likely explanation because the expansion of *P. falciparum* and subsequent impacts on human selection likely began in the last 10,000 years (Joy et al., 2003).

To assess whether the E756del variant is derived (i.e., is a new allele that occurred in Africans) or ancestral, we investigated the architecture of the *PIEZO1* locus in the archaic humans and non-human primates. There is low amino acid sequence homology near the E756del locus between humans and non-human primates (Figure S4A); thus, we could not investigate pre-human ancestry. We found, however, that both Neanderthals and Denisovans had the wild-type E756 in their *PIEZO1* genes (Figures 6C and S4B). This finding shows that the *PIEZO1* E756del gain-of-function allele is derived in individuals of African descent, again consistent with being under positive selection (Sabeti et al., 2006). Combined, our analyses show that the *PIEZO1* gain-of-function mutation E756del is a high-frequency (present in one-third of African population) derived allele that is highly differentiated in populations where malaria is endemic. These findings are highly suggestive of the E756del genetic variant being under positive selection in populations of African descent (Sabeti et al., 2006), presumably because of its likely role as a malaria-protective allele.

RBCs from E756del African American Carriers Are Dehydrated and Cause Reduced Infection by *Plasmodium falciparum In Vitro*

We acquired blood samples from healthy volunteer African American donors and tested whether E756del causes xerocytosis-like RBC dehydration and, importantly, whether it confers attenuation of infection against *P. falciparum in vitro*. We obtained 25 whole-blood samples and used white blood cells to sequence the exon containing E756del. We found that nine (36%) African American donors were heterozygous for E756del (none were homozygous) (Figure S5A). We also screened all 25 donors for other known common mutations that affect RBC morphology and could potentially influence susceptibility to *Plasmodium* infection. Our sequencing results showed that all 25 donors were free of HbS, HbC, and HbE mutations in the β-globin chains that cause hemoglobinopathy (Figure S5B). In addition, we showed that none of the 25 donors had the variations that cause α-thalassemia (Figure S5C), another condition associated with RBC abnormality and *Plasmodium* infection (Chong et al., 2000).

Next, we imaged RBCs with scanning electron microscopy from three carriers and showed that all had RBCs with echinocyte and stomatocyte morphologies, which is a characteristic of hereditary xerocytosis RBCs (Figure 7A). Remarkably, we also found that RBCs from all 9 donors with the E756del mutation were dehydrated as assayed by osmotic fragility test (Figures 7B and 7C), similar to RBCs from known xerocytosis patients (Delaunay, 2004; Archer et al., 2014). Next, we infected both control and E756del carrier RBCs with *P. falciparum in vitro*. Parasitemia was significantly lower for E756del carriers relative to non-carriers, measured by both Giemsa and SYBR green staining methods (Figures 7D and 7E) (Johnson et al., 2007).

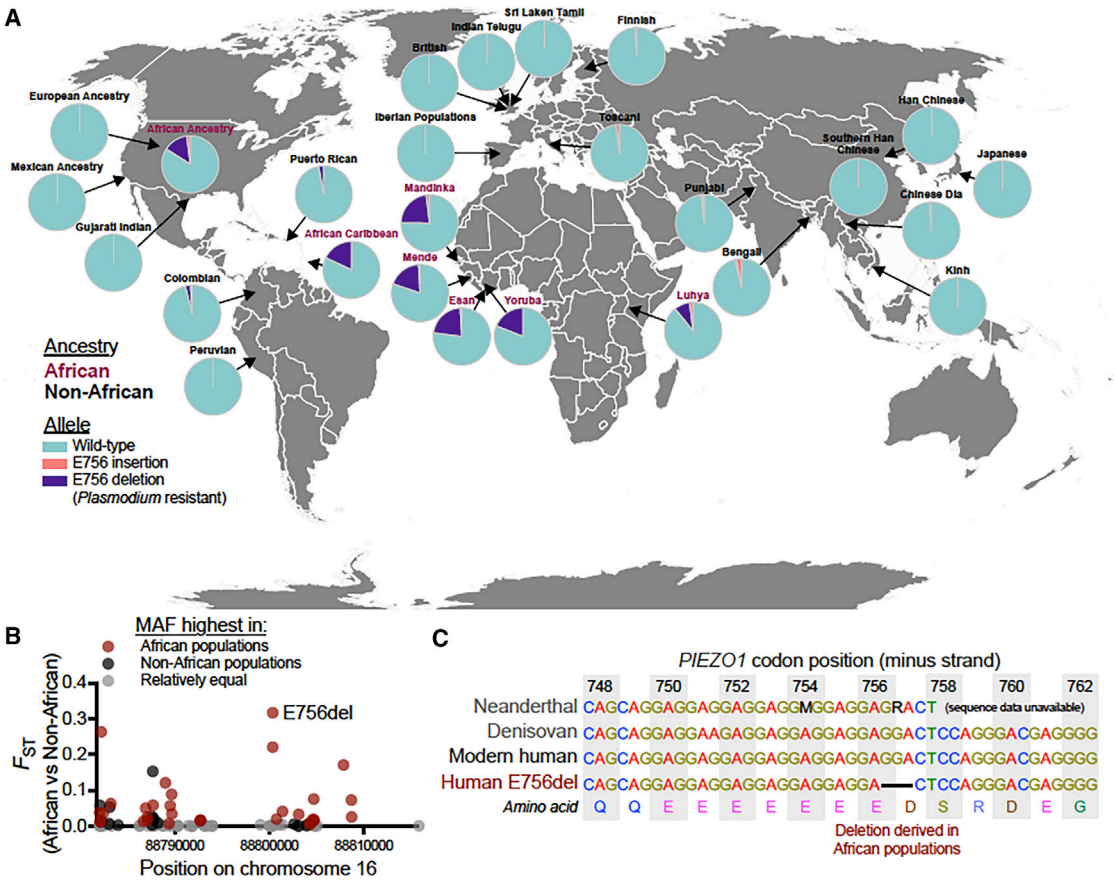

Figure 6. Population Genetics of *PIEZO1* Gain-of-Function E756del Allele Common in Populations of African Descent

(A) Human population demographics for E756 indels. E756 deletion (TCC/–) exists at high frequencies in all populations of African descents (purple). A minor allele, E756 insertion (TCC/TCCTCC) was also discovered (coral).

(B) Differentiation (F_{ST}) between populations of African and non-African ancestry at each loci for all *PIEZO1* missense mutations. Alleles are colored by whether the minor allele frequency (MAF) was highest in African (red) or non-African (black) populations, or were similar (gray).

(C) A nucleotide alignment of modern and pre-modern (Neanderthal and Denisovan) human *PIEZO1* minus strand sequences around the E756del allele showing the codon positions. (Ambiguous base: M = C or A; R = A or G). The TCC deletion (GGA on minus strand) spans two codons but only deletes E756 while shifting nucleotides to leave D757 intact. Individual Neanderthal and Denisovan reads used to create this alignment and comparisons to non-human primate PIEZO1 amino acid sequences are shown in Figure S4.

See also Figure S4.

Together, our data demonstrate that E756del is a common PIEZO1 gain-of-function mutation in African populations, causing RBC dehydration in otherwise healthy African Americans, and is likely under positive selection, due to its ability to confer reduced susceptibility of RBCs to *P. falciparum* infection.

DISCUSSION

Gain-of-Function *Piezo1* Expression in Blood Cells Provides Protection against *Plasmodium*-Induced Cerebral Complications *In Vivo*

Dehydrated RBCs, including those from hereditary xerocytosis patients, show slower infection rates to *P. falciparum in vitro* (Tiffert et al., 2005). However, this mechanism of protection has never been tested *in vivo*. To address these issues, we engineered a gain-of-function Piezo1 mouse that recapitulated most features of hereditary xerocytosis. Remarkably, gain-of-function Piezo1 mutation induced in different types of blood cells caused dramatic shifts in survival rates in response to *P. berghei* infection, caused by reduced parasite growth rate of blood stage as well as protection from experimental cerebral malaria.

Our mouse genetic data suggest that gain-of-function Piezo1-induced RBC dehydration is a major determinant in the protection against cerebral complications of malaria. Several other genetic mutations that affect RBC morphology are associated with resistance to malaria in human populations (Hedrick, 2004; Feng et al., 2004), and some of these mutations also cause RBC dehydration, such as sickle cell disease (Brugnara, 1995). Similar experiments can be performed in the future to evaluate the potential contribution of RBC dehydration to malaria resistance in the genetic disorders mentioned above. Another important next step is to determine the molecular mechanisms responsible for RBC-dehydration-dependent attenuation of *Plasmodium* infection.

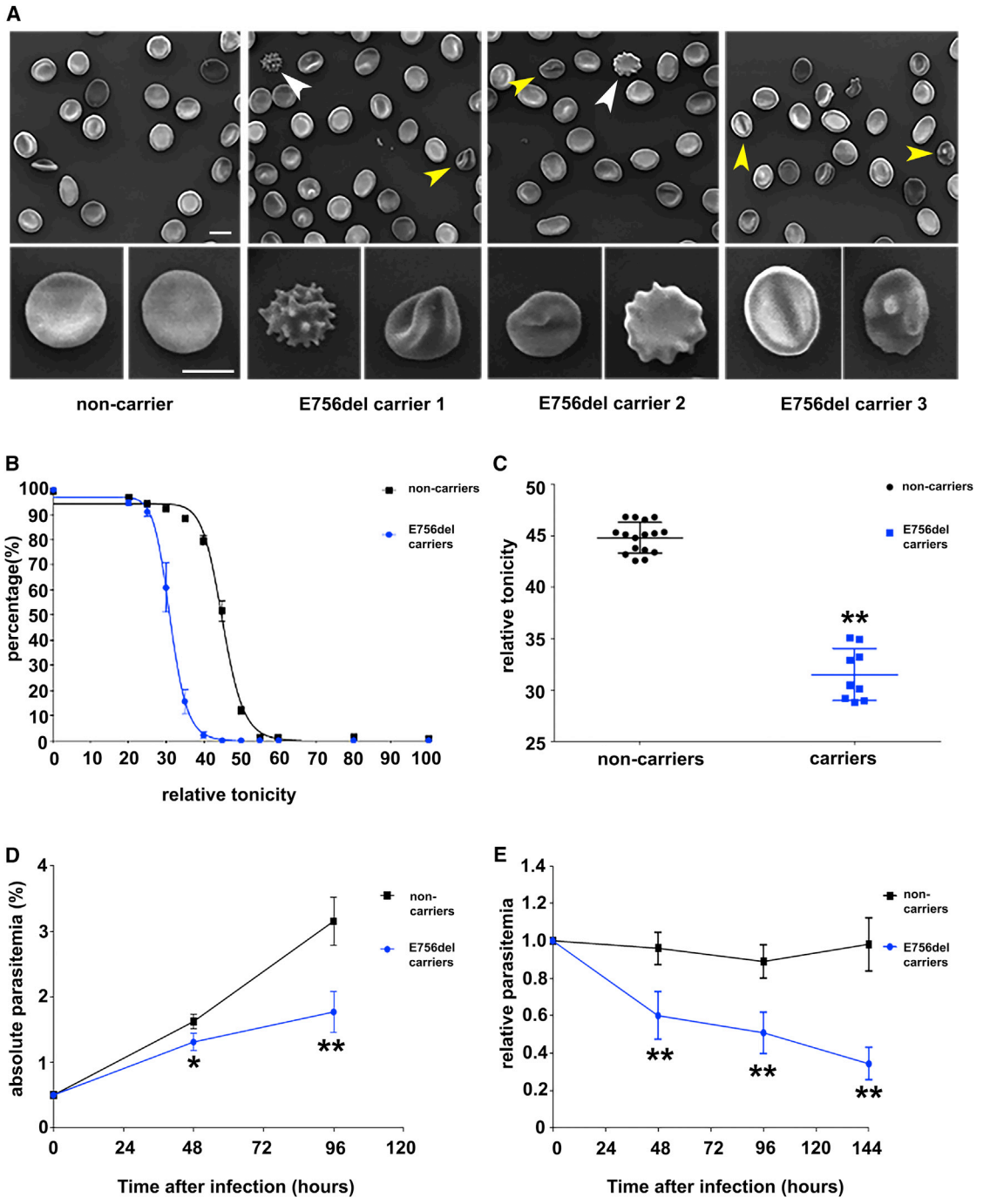

Figure 7. Characterization of RBCs from E756del Carriers for Xerocytosis-like Phenotypes and *P. falciparum* Infection

(A) SEM images. Three individual E756del carriers have RBCs with echinocytes (white arrowhead) and stomatocytes (yellow arrowhead), magnified in lower panels. Scale bar for upper panels, 10 μm; for lower panels, 5 μm.

(B and C) Osmotic fragility test. RBCs from E756del heterozygous carriers (n = 9) had a left-shifted curve (blue) compared to controls (n = 16) (black) (B), as quantified in (C) $^{**}p < 0.01$.

(D and E) *P. falciparum* infection into RBCs from E756del carriers. Giemsa staining (D) and SYBR Green labeling of parasite DNA inside RBCs (E) ($^{**}p < 0.01$, $^{*}p < 0.05$).

Statistics: Student's t test for each time point. Data are presented as means ± SEM. See also Figure S5.

In addition to RBC dehydration, we discovered an unexpected function of gain-of-function PIEZO1 in immune cells during *Plasmodium* infection. T cells play both pathogenic and protective roles in human malaria, as well as in murine malaria models (Hafalla et al., 2006; Ewer et al., 2013). T cells experience diverse mechanical stimuli during development and function, but the role of mechanosensitive ion channels in immune cells is poorly understood (Huse, 2017). It is possible that overactive PIEZO1 channels alter T cell developmental programs and/or modulate their activity when encountering parasites. It will be of interest to use both gain-of-function and loss-of-function Piezo1 mice to explore the role of this ion channel in T cells.

The Discovery of Gain-of-Function *PIEZO1* Allele Present in One-Third of the African Population

The discovery of gain-of-function PIEZO1 E756del in African populations with a high allele frequency of ~18% (such that an estimated one-third of African people carry this mutation as heterozygotes) is quite surprising. Our findings dramatically redefine the epidemiology of this disorder: hereditary xerocytosis-like condition is much more common than previously anticipated. Thus, E756del provides a unique opportunity to evaluate the association between gain-of-function PIEZO1, RBC dehydration, and malaria in endemic regions.

Despite the experimental evidence above, PIEZO1 locus was not detected as a strong candidate by recent genome-wide association studies (GWASs) that aimed to identify genetic loci for severe malaria resistance (Leffler et al., 2017). This is potentially due to GWAS limitations and the complexity of this particular genetic locus. GWAS samples have high levels of genetic diversity and are underrepresented in reference panels of genetic variation (Malaria Genomic Epidemiology Network, 2014; Leffler et al., 2017). Also, GWASs mainly use SNPs to determine association, and this would be challenging to evaluate more complex loci without genetic imputation method. E756del is in such a locus with multiple short tandem repeats (Figure 6C), so that imputation of this mutation into current GWAS datasets is not straightforward. In this regard, our experimental data provide promising clues for association analysis: sequencing this particular locus in endemic population can determine whether E756del is associated with protection against severe malaria.

E756del Provides an Opportunity to Evaluate the Role of Overactive Mechanotransduction in Human Health

Does E756del allele cause hereditary xerocytosis and other disorders? We readily identified E756del carriers from self-reported healthy African American blood donors. Whether E756del carriers have anemia or splenomegaly is not known to date. A full clinical evaluation of individuals carrying this allele will be of high interest to assess how overactive PIEZO1 influences xerocytosis-related phenotypes, as well as other conditions. For example, analysis of loss-of-function *Piezo1* mice has demonstrated a critical role of this ion channel in cardiovascular function (Retailleau et al., 2015; Wang et al., 2016; Rode et al., 2017). Therefore, it will be of interest to assess the role of overactive PIEZO1 channel in hypertension, which has high incidence in African Americans (Kaplan, 1994). We expect that a complete clinical characterization of individuals with the E756del allele will shed further light on the range of phenotypes that are associated with *PIEZO1*, including anemia, splenomegaly, autoimmune diseases, various aspects of cardiovascular function, as well as in indications not previously associated with PIEZO1.

STAR★METHODS

Detailed methods are provided in the online version of this paper and include the following:

- KEY RESOURCES TABLE
- CONTACT FOR REAGENT AND RESOURCE SHARING
- EXPERIMENTAL MODEL AND SUBJECT DETAILS
  - Mice
  - Cell lines and cell culture
  - Human blood samples
- METHOD DETAILS
  - P. berghei infections and parasitemia measurement by flow cytometry
  - Blood-brain barrier and experimental cerebral malaria assay
  - Scanning Electron Microscope
  - Osmotic fragility test and hematology test
  - Gain-of-function Piezo1 mice generation
  - Mechanical stimulation
  - Cell culture and transient transfection
  - Fluorescent imaging plate reader (384-well format)
  - Real time quantitative PCR.
  - CD4+ and CD8+ T cell isolation
  - Population genetic analysis
  - Genotyping in African American blood donors
  - P. falciparum culture
  - Parasitemia Determination
- QUANTIFICATION AND STATISTICAL ANALYSIS
  - Statistical analysis

SUPPLEMENTAL INFORMATION

Supplemental Information includes five figures and two tables and can be found with this article online at https://doi.org/10.1016/j.cell.2018.02.047.

ACKNOWLEDGMENTS

We thank Ali Torkamani for advice on genomics, Dominic Kwiatkowski and Ilya Shlyakhter for discussions, and Lisa Stowers for reading the manuscript. This work was partly supported by NIH grants R01 DE022358 to A.P. and AI090141 and AI103058 to E.A.W. S.M. is supported by a Calibr-GHDDI Gates postdoctoral fellowship. G.L. is supported by an A.P. Giannini postdoctoral fellowship. K.G.A. is a Pew Biomedical Scholar and is supported by NIH NCATS CTSA UL1TR001114. A.P. is an investigator of the Howard Hughes Medical Institute.

AUTHOR CONTRIBUTIONS

A.P. and S.M. designed experiments and wrote the paper. S.M., S.C., and M.L. performed animal experiments and flow cytometry. S.M. performed human blood analysis. G.L., E.P., and E.A.W. performed and analyzed the *P. falciparum* infection experiment. N.D.G. and K.G.A. analyzed population genetics data and wrote those sections. W.Z. and S.E.M. performed electrophysiological experiments. R.G. and A.I.S. performed bioinformatics analysis. S.E.M. and V.L. carried out screening. S.C., S.M., and T.W. performed

molecular cloning. S.M.K. and C.J.J. made reagents. R.L., L.B., M.B., C.S., K.W., E.H., E.A.W., and K.G.A. all contributed conceptually.

DECLARATION OF INTERESTS

The authors declare no competing interests.

Received: October 4, 2017
Revised: January 6, 2018
Accepted: February 14, 2018
Published: March 22, 2018

REFERENCES

Albuisson, J., Murthy, S.E., Bandell, M., Coste, B., Louis-Dit-Picard, H., Mathur, J., Fénéant-Thibault, M., Tertian, G., de Jaureguiberry, J.-P., Syfuss, P.-Y., et al. (2013). Dehydrated hereditary stomatocytosis linked to gain-of-function mutations in mechanically activated PIEZO1 ion channels. Nat. Commun. *4*, 1884.

Archer, N.M., Shmukler, B.E., Andolfo, I., Vandorpe, D.H., Gnanasambandam, R., Higgins, J.M., Rivera, A., Fleming, M.D., Sachs, F., Gottlieb, P.A., et al. (2014). Hereditary xerocytosis revisited. Am. J. Hematol. *89*, 1142–1146.

Auton, A., Brooks, L.D., Durbin, R.M., Garrison, E.P., Kang, H.M., Korbel, J.O., Marchini, J.L., McCarthy, S., McVean, G.A., and Abecasis, G.R.; 1000 Genomes Project Consortium (2015). A global reference for human genetic variation. Nature *526*, 68–74.

Bae, C., Gnanasambandam, R., Nicolai, C., Sachs, F., and Gottlieb, P.A. (2013). Xerocytosis is caused by mutations that alter the kinetics of the mechanosensitive channel PIEZO1. Proc. Natl. Acad. Sci. USA *110*, E1162–E1168.

Baptista, F.G., Pamplona, A., Pena, A.C., Mota, M.M., Pied, S., and Vigário, A.M. (2010). Accumulation of Plasmodium berghei-infected red blood cells in the brain is crucial for the development of cerebral malaria in mice. Infect. Immun. *78*, 4033–4039.

Belnoue, E., Kayibanda, M., Vigario, A.M., Deschemin, J.-C., van Rooijen, N., Viguier, M., Snounou, G., and Rénia, L. (2002). On the pathogenic role of brain-sequestered alphabeta CD8+ T cells in experimental cerebral malaria. J. Immunol. *169*, 6369–6375.

Brugnara, C. (1995). Erythrocyte dehydration in pathophysiology and treatment of sickle cell disease. Curr. Opin. Hematol. *2*, 132–138.

Cahalan, S.M., Lukacs, V., Ranade, S.S., Chien, S., Bandell, M., and Patapoutian, A. (2015). Piezo1 links mechanical forces to red blood cell volume. eLife. Published online May 22, 2015. https://doi.org/10.7554/eLife.07370.

Chen, T.-W., Wardill, T.J., Sun, Y., Pulver, S.R., Renninger, S.L., Baohan, A., Schreiter, E.R., Kerr, R.A., Orger, M.B., Jayaraman, V., et al. (2013). Ultrasensitive fluorescent proteins for imaging neuronal activity. Nature *499*, 295–300.

Chesler, A.T., Szczot, M., Bharucha-Goebel, D., Čeko, M., Donkervoort, S., Laubacher, C., Hayes, L.H., Alter, K., Zampieri, C., Stanley, C., et al. (2016). The role of PIEZO2 in human mechanosensation. N. Engl. J. Med. *375*, 1355–1364.

Chong, S.S., Boehm, C.D., Higgs, D.R., and Cutting, G.R. (2000). Single-tube multiplex-PCR screen for common deletional determinants of alpha-thalassemia. Blood *95*, 360–362.

Chua, C.L.L., Brown, G., Hamilton, J.A., Rogerson, S., and Boeuf, P. (2013). Monocytes and macrophages in malaria: Protection or pathology? Trends Parasitol. *29*, 26–34.

Clausen, B.E., Burkhardt, C., Reith, W., Renkawitz, R., and Förster, I. (1999). Conditional gene targeting in macrophages and granulocytes using LysMcre mice. Transgenic Res. *8*, 265–277.

Coste, B., Mathur, J., Schmidt, M., Earley, T.J., Ranade, S., Petrus, M.J., Dubin, A.E., and Patapoutian, A. (2010). Piezo1 and Piezo2 are essential components of distinct mechanically activated cation channels. Science *330*, 55–60.

de Boer, J., Williams, A., Skavdis, G., Harker, N., Coles, M., Tolaini, M., Norton, T., Williams, K., Roderick, K., Potocnik, A.J., and Kioussis, D. (2003). Transgenic mice with hematopoietic and lymphoid specific expression of Cre. Eur. J. Immunol. *33*, 314–325.

de Oca, M.M., Engwerda, C., and Haque, A. (2013). Plasmodium berghei ANKA (PbA) infection of C57BL/6J mice: A model of severe malaria. Methods Mol. Biol. *1031*, 203–213.

de Souza, J.B., Hafalla, J.C.R., Riley, E.M., and Couper, K.N. (2010). Cerebral malaria: Why experimental murine models are required to understand the pathogenesis of disease. Parasitology *137*, 755–772.

Delaunay, J. (2004). The hereditary stomatocytoses: Genetic disorders of the red cell membrane permeability to monovalent cations. Semin. Hematol. *41*, 165–172.

Dubin, A.E., Murthy, S., Lewis, A.H., Brosse, L., Cahalan, S.M., Grandl, J., Coste, B., and Patapoutian, A. (2017). Endogenous Piezo1 can confound mechanically activated channel identification and characterization. Neuron *94*, 266–270.

Dunst, J., Kamena, F., and Matuschewski, K. (2017). Cytokines and chemokines in cerebral malaria pathogenesis. Front. Cell. Infect. Microbiol. *7*, 324.

Elias, J.M., and Greene, C. (1979). Modified Steiner method for the demonstration of spirochetes in tissue. Am. J. Clin. Pathol. *71*, 109–111.

Ewer, K.J., O'Hara, G.A., Duncan, C.J.A., Collins, K.A., Sheehy, S.H., Reyes-Sandoval, A., Goodman, A.L., Edwards, N.J., Elias, S.C., Halstead, F.D., et al. (2013). Protective CD8+ T-cell immunity to human malaria induced by chimpanzee adenovirus-MVA immunisation. Nat. Commun. *4*, 2836.

Feng, Z., Smith, D.L., McKenzie, F.E., and Levin, S.A. (2004). Coupling ecology and evolution: Malaria and the S-gene across time scales. Math. Biosci. *189*, 1–19.

Ferreira, A., Marguti, I., Bechmann, I., Jeney, V., Chora, A., Palha, N.R., Rebelo, S., Henri, A., Beuzard, Y., and Soares, M.P. (2011). Sickle hemoglobin confers tolerance to Plasmodium infection. Cell *145*, 398–409.

Franke-Fayard, B., Trueman, H., Ramesar, J., Mendoza, J., van der Keur, M., van der Linden, R., Sinden, R.E., Waters, A.P., and Janse, C.J. (2004). A Plasmodium berghei reference line that constitutively expresses GFP at a high level throughout the complete life cycle. Mol. Biochem. Parasitol. *137*, 23–33.

Glogowska, E., Schneider, E.R., Maksimova, Y., Schulz, V.P., Lezon-Geyda, K., Wu, J., Radhakrishnan, K., Keel, S.B., Mahoney, D., Freidmann, A.M., et al. (2017). Novel mechanisms of PIEZO1 dysfunction in hereditary xerocytosis. Blood *130*, 1845–1856.

Hafalla, J.C.R., Cockburn, I.A., and Zavala, F. (2006). Protective and pathogenic roles of CD8+ T cells during malaria infection. Parasite Immunol. *28*, 15–24.

Hedrick, P. (2004). Estimation of relative fitnesses from relative risk data and the predicted future of haemoglobin alleles S and C. J. Evol. Biol. *17*, 221–224.

Heinrich, A.C., Pelanda, R., and Klingmüller, U. (2004). A mouse model for visualization and conditional mutations in the erythroid lineage. Blood *104*, 659–666.

Howland, S.W., Claser, C., Poh, C.M., Gun, S.Y., and Rénia, L. (2015). Pathogenic CD8+ T cells in experimental cerebral malaria. Semin. Immunopathol. *37*, 221–231.

Hunt, N.H., Grau, G.E., Engwerda, C., Barnum, S.R., van der Heyde, H., Hansen, D.S., Schofield, L., and Golenser, J. (2010). Murine cerebral malaria: The whole story. Trends Parasitol. *26*, 272–274.

Hunt, N.H., Ball, H.J., Hansen, A.M., Khaw, L.T., Guo, J., Bakmiwewa, S., Mitchell, A.J., Combes, V., and Grau, G.E.R. (2014). Cerebral malaria: gamma-interferon redux. Front. Cell. Infect. Microbiol. *4*, 113.

Huse, M. (2017). Mechanical forces in the immune system. Nat. Rev. Immunol. *17*, 679–690.

Johnson, J.D., Dennull, R.A., Gerena, L., Lopez-Sanchez, M., Roncal, N.E., and Waters, N.C. (2007). Assessment and continued validation of the malaria SYBR green I-based fluorescence assay for use in malaria drug screening. Antimicrob. Agents Chemother. *51*, 1926–1933.

Joy, D.A., Feng, X., Mu, J., Furuya, T., Chotivanich, K., Krettli, A.U., Ho, M., Wang, A., White, N.J., Suh, E., et al. (2003). Early origin and recent expansion of Plasmodium falciparum. Science *300*, 318–321.

Kaplan, N.M. (1994). Ethnic aspects of hypertension. Lancet *344*, 450–452.

Katoh, K., Misawa, K., Kuma, K., and Miyata, T. (2002). MAFFT: A novel method for rapid multiple sequence alignment based on fast Fourier transform. Nucleic Acids Res. *30*, 3059–3066.

Kent, W.J., Sugnet, C.W., Furey, T.S., Roskin, K.M., Pringle, T.H., Zahler, A.M., and Haussler, D. (2002). The human genome browser at UCSC. Genome Res. *12*, 996–1006.

Kwiatkowski, D.P. (2005). How malaria has affected the human genome and what human genetics can teach us about malaria. Am. J. Hum. Genet. *77*, 171–192.

Lambros, C., and Vanderberg, J.P. (1979). Synchronization of Plasmodium falciparum erythrocytic stages in culture. J. Parasitol. *65*, 418–420.

Leffler, E.M., Band, G., Busby, G.B.J., Kivinen, K., Le, Q.S., Clarke, G.M., Bojang, K.A., Conway, D.J., Jallow, M., Sisay-Joof, F., et al.; Malaria Genomic Epidemiology Network (2017). Resistance to malaria through structural variation of red blood cell invasion receptors. Science. Published online June 16, 2017. https://doi.org/10.1126/science.aam6393.

Lek, M., Karczewski, K.J., Minikel, E.V., Samocha, K.E., Banks, E., Fennell, T., O'Donnell-Luria, A.H., Ware, J.S., Hill, A.J., Cummings, B.B., et al.; Exome Aggregation Consortium (2016). Analysis of protein-coding genetic variation in 60,706 humans. Nature *536*, 285–291.

Li, J., Hou, B., Tumova, S., Muraki, K., Bruns, A., Ludlow, M.J., Sedo, A., Hyman, A.J., McKeown, L., Young, R.S., et al. (2014). Piezo1 integration of vascular architecture with physiological force. Nature *515*, 279–282.

Loy, D.E., Liu, W., Li, Y., Learn, G.H., Plenderleith, L.J., Sundararaman, S.A., Sharp, P.M., and Hahn, B.H. (2017). Out of Africa: Origins and evolution of the human malaria parasites Plasmodium falciparum and Plasmodium vivax. Int. J. Parasitol. *47*, 87–97.

Lukacs, V., Mathur, J., Mao, R., Bayrak-Toydemir, P., Procter, M., Cahalan, S.M., Kim, H.J., Bandell, M., Longo, N., Day, R.W., et al. (2015). Impaired PIEZO1 function in patients with a novel autosomal recessive congenital lymphatic dysplasia. Nat. Commun. *6*, 8329.

Maher, A.D., and Kuchel, P.W. (2003). The Gárdos channel: A review of the Ca2+-activated K+ channel in human erythrocytes. Int. J. Biochem. Cell Biol. *35*, 1182–1197.

Malaria Genomic Epidemiology Network (2014). Reappraisal of known malaria resistance loci in a large multicenter study. Nat. Genet. *46*, 1197–1204.

Meyer, M., Kircher, M., Gansauge, M.-T., Li, H., Racimo, F., Mallick, S., Schraiber, J.G., Jay, F., Prüfer, K., de Filippo, C., et al. (2012). A high-coverage genome sequence from an archaic Denisovan individual. Science *338*, 222–226.

Murthy, S.E., Dubin, A.E., and Patapoutian, A. (2017). Piezos thrive under pressure: Mechanically activated ion channels in health and disease. Nat. Rev. Mol. Cell Biol. *18*, 771–783.

Nacer, A., Movila, A., Sohet, F., Girgis, N.M., Gundra, U.M., Loke, P., Daneman, R., and Frevert, U. (2014). Experimental cerebral malaria pathogenesis–hemodynamics at the blood brain barrier. PLoS Pathog. *10*, e1004528.

Phillips, R.E., and Pasvol, G. (1992). Anaemia of Plasmodium falciparum malaria. Baillieres Clin. Haematol. *5*, 315–330.

Ranade, S.S., Woo, S.-H., Dubin, A.E., Moshourab, R.A., Wetzel, C., Petrus, M., Mathur, J., Bégay, V., Coste, B., Mainquist, J., et al. (2014a). Piezo2 is the major transducer of mechanical forces for touch sensation in mice. Nature *516*, 121–125.

Ranade, S.S., Qiu, Z., Woo, S.-H., Hur, S.S., Murthy, S.E., Cahalan, S.M., Xu, J., Mathur, J., Bandell, M., Coste, B., et al. (2014b). Piezo1, a mechanically activated ion channel, is required for vascular development in mice. Proc. Natl. Acad. Sci. USA *111*, 10347–10352.

Ranade, S.S., Syeda, R., and Patapoutian, A. (2015). Mechanically activated ion channels. Neuron *87*, 1162–1179.

Reich, D., Green, R.E., Kircher, M., Krause, J., Patterson, N., Durand, E.Y., Viola, B., Briggs, A.W., Stenzel, U., Johnson, P.L.F., et al. (2010). Genetic history of an archaic hominin group from Denisova Cave in Siberia. Nature *468*, 1053–1060.

Retailleau, K., Duprat, F., Arhatte, M., Ranade, S.S., Peyronnet, R., Martins, J.R., Jodar, M., Moro, C., Offermanns, S., Feng, Y., et al. (2015). Piezo1 in smooth muscle cells is involved in hypertension-dependent arterial remodeling. Cell Rep. *13*, 1161–1171.

Rode, B., Shi, J., Endesh, N., Drinkhill, M.J., Webster, P.J., Lotteau, S.J., Bailey, M.A., Yuldasheva, N.Y., Ludlow, M.J., Cubbon, R.M., et al. (2017). Piezo1 channels sense whole body physical activity to reset cardiovascular homeostasis and enhance performance. Nat. Commun. *8*, 350.

Sabeti, P.C., Schaffner, S.F., Fry, B., Lohmueller, J., Varilly, P., Shamovsky, O., Palma, A., Mikkelsen, T.S., Altshuler, D., and Lander, E.S. (2006). Positive natural selection in the human lineage. Science *312*, 1614–1620.

Schwenk, F., Baron, U., and Rajewsky, K. (1995). A cre-transgenic mouse strain for the ubiquitous deletion of loxP-flanked gene segments including deletion in germ cells. Nucleic Acids Res. *23*, 5080–5081.

Syeda, R., Xu, J., Dubin, A.E., Coste, B., Mathur, J., Huynh, T., Matzen, J., Lao, J., Tully, D.C., Engels, I.H., et al. (2015). Chemical activation of the mechanotransduction channel Piezo1. eLife. Published online May 22, 2015. https://doi.org/10.7554/eLife.07370.

Tiffert, T., Lew, V.L., Ginsburg, H., Krugliak, M., Croisille, L., and Mohandas, N. (2005). The hydration state of human red blood cells and their susceptibility to invasion by Plasmodium falciparum. Blood *105*, 4853–4860.

Trager, W., and Jensen, J.B. (1976). Human malaria parasites in continuous culture. Science *193*, 673–675.

Vacchio, M.S., Wang, L., Bouladoux, N., Carpenter, A.C., Xiong, Y., Williams, L.C., Wohlfert, E., Song, K.-D., Belkaid, Y., Love, P.E., and Bosselut, R. (2014). A ThPOK-LRF transcriptional node maintains the integrity and effector potential of post-thymic CD4+ T cells. Nat. Immunol. *15*, 947–956.

Vitti, J.J., Grossman, S.R., and Sabeti, P.C. (2013). Detecting natural selection in genomic data. Annu. Rev. Genet. *47*, 97–120.

Wang, S., Chennupati, R., Kaur, H., Iring, A., Wettschureck, N., and Offermanns, S. (2016). Endothelial cation channel PIEZO1 controls blood pressure by mediating flow-induced ATP release. J. Clin. Invest. *126*, 4527–4536.

Woo, S.-H., Ranade, S., Weyer, A.D., Dubin, A.E., Baba, Y., Qiu, Z., Petrus, M., Miyamoto, T., Reddy, K., Lumpkin, E.A., et al. (2014). Piezo2 is required for Merkel-cell mechanotransduction. Nature *509*, 622–626.

Woo, S.-H., Lukacs, V., de Nooij, J.C., Zaytseva, D., Criddle, C.R., Francisco, A., Jessell, T.M., Wilkinson, K.A., and Patapoutian, A. (2015). Piezo2 is the principal mechanotransduction channel for proprioception. Nat. Neurosci. *18*, 1756–1762.

Yañez, D.M., Manning, D.D., Cooley, A.J., Weidanz, W.P., and van der Heyde, H.C. (1996). Participation of lymphocyte subpopulations in the pathogenesis of experimental murine cerebral malaria. J. Immunol. *157*, 1620–1624.

Zarychanski, R., Schulz, V.P., Houston, B.L., Maksimova, Y., Houston, D.S., Smith, B., Rinehart, J., and Gallagher, P.G. (2012). Mutations in the mechanotransduction protein PIEZO1 are associated with hereditary xerocytosis. Blood *120*, 1908–1915.

STAR★METHODS

KEY RESOURCES TABLE

REAGENT or RESOURCE	SOURCE	IDENTIFIER
Biological Samples		
Healthy whole blood samples	TSRI normal blood donor service (La Jolla, CA)	https://nbds.scripps.edu/
Healthy whole blood samples	biological specialty corporation (PA)	http://www.biospecialty.com/
Bacterial and Virus Strains		
Mach1 competent cells	Thermo Fisher	Catalog#C862003
Chemicals, Peptides, and Recombinant Proteins		
Yoda1 (50mg stock) (Tocris)	Fisher Scientific	Catalog#5586/50
Critical Commercial Assays		
MojoSort mouse CD4 T cell Nanobeads kit	BioLegend (San Diego,CA)	Catalog#480069
MojoSort mouse CD8 T cell Nanobeads kit	BioLegend (San Diego,CA)	Catalog#480007
QIAamp DNA blood mini kit	QIAGEN	Catalog#51104
Quick-RNA Whole Blood	Zymo Research, Irvine, CA	Catalog#R1201
GoTaq qPCR Master Mix	Promega, Madison	Catalog#A6002
Experimental Models: Cell Lines		
Human *Piezo1*KO HEK cells	Our own lab	Dubin et al., 2017
Experimental Models: Organisms/Strains		
Mouse: B6N.Cg-Tg(Vav1-icre)A2Kio/J	The Jackson Lab	Stock# 018968
Mouse: B6;129S1-*Kcnn4*^{tm1Jemn}/J	The Jackson Lab	Stock# 018826
Mouse: B6.C-Tg(CMV-cre)1Cgn/J	The Jackson Lab	Stock# 006054
Mouse: C57BL/6-Tg(CD2-cre)1Lov/J	The Jackson Lab	Stock# 027406
Mouse: B6.129P2-*Lyz2*$^{tm1(cre)Ifo}$/J	The Jackson Lab	Stock# 004781
Mouse: Epor$^{tm1(EGFP/cre)Uk}$	Dr. Klingmuller group at Max-Planck-Institute für Immunbiologie, Freiburg, Germany	N/A
Mouse: Piezo1cx/cx	Taconic Biosciences	Customized
Plasmodium Berghei: *P. berghei* (ANKA) GFPcon 259cl2	California Institute for Biomedical Research, La Jolla, USA	N/A
Plasmodium Berghei: *P. berghei* (ANKA) mCherry-hsp70-Luc-eef1a	Leiden Malaria Research Group, the Netherlands	line 1868
Plasmodium falciparum	Elizabeth Winzeler, university of California, San Diego	N/A
Oligonucleotides		
CTCACAGACAGGTGTTCATC	This paper	RT-PCR for mouse Piezo1 mRNA
GCAAACTCACGTCAAGGAGA	This paper	RT-PCR for mouse Piezo1 mRNA
GCACCACCAACTGCTTAG	This paper	RT-PCR for mouse gapdh mRNA
GGATGCAGGGATGATGTTC	This paper	RT-PCR for mouse gapdh mRNA
AGAAGAGCCAAGGACAGGTA	This paper	Human E756del amplicon
TTGCAGCCTCACCTTCTTTC	This paper	Human E756del amplicon
CCCCTCGCCAAGTCCACCC	Chong et al., 2000	α-thalassemia a2/3.7-F
AAAGCACTCTAGGGTCCAGCG	Chong et al., 2000	α-thalassemia 3.7/20.5-R
AGACCAGGAAGGGCCGGTG	Chong et al., 2000	α-thalassemia a2-R
GGTTTACCCATGTGGTGCCTC	Chong et al., 2000	α-thalassemia 4.2-F
CCCGTTGGATCTTCTCATTTCCC	Chong et al., 2000	α-thalassemia 4.2-R
CGATCTGGGCTCTGTGTTCTC	Chong et al., 2000	α-thalassemia SEA-F
AGCCCACGTTGTGTTCATGGC	Chong et al., 2000	α-thalassemia SEA-R

(*Continued on next page*)

Continued		
REAGENT or RESOURCE	SOURCE	IDENTIFIER
TGCAAATATGTTTCTCTCATTCTGTG	Chong et al., 2000	α-thalassemia FIL-F
ATAACCTTTATCTGCCACATGTAGC	Chong et al., 2000	α-thalassemia FIL-R
GCCCAACATCCGGAGTACATG	Chong et al., 2000	α-thalassemia 20.5-F
TACCCTTTGCAAGCACACGTAC	Chong et al., 2000	α-thalassemia MED-F
TCAATCTCCGACAGCTCCGAC	Chong et al., 2000	α-thalassemia MED-R
Recombinant DNA		
Plasmid: 3.2pc-IRES-tdTomato	This paper	N/A
Software and Algorithms		
Prism7	GraphPad software	https://www.graphpad.com
Geneious	Geneious	https://www.geneious.com/

CONTACT FOR REAGENT AND RESOURCE SHARING

Further information and requests for resources and reagents should be directed to and will be fulfilled by the Lead Contact, Ardem Patapoutian (ardem@scripps.edu).

EXPERIMENTAL MODEL AND SUBJECT DETAILS

All animal procedures were approved by the Institutional Animal Care and Use Committees of The Scripps Research Institute (TSRI).

Mice

*Piezo1*GOF ^{blood}, *Piezo1*GOF ^{constitutive}, *Piezo1*GOF $^{T\ cells}$, *Piezo1*GOF ^{macrophage,} and *Piezo1*GOF ^{RBC} mice were generated by breeding *Piezo1*cx/cx with vav1-cre (The Jackson Laboratory, stock# 018968) and cmv-cre (The Jackson Laboratory stock# 006054), hCD2-cre (The Jackson Laboratory stock# 027406), LysM-cre (The Jackson Laboratory stock# 004781), and EpoR-cre (a gift from Dr. Klingmuller group at Max-Planck-Institute für Immunbiologie, Freiburg, Germany). *KCa3.1* −/− mice were ordered from The Jackson Laboratory (stock# 018826). Gain-of-function *Piezo1* mice were generated and maintained on C57BL/6 background. All animals were backcrossed at least 10 generations to C57BL/6. The mice were housed in a 12hr light/dark cycle (light from 6am to 6pm) in a temperature-controlled room (24 degree) with free access to food and water. The ages and sexes of mice are indicated in the following method section. Littermates were used for experiments.

Cell lines and cell culture

*PIEZO1*KO HEK cells were grown in Dulbecco's modified Eagle's medium containing 4.5 mg/ml glucose, 10% fetal bovine serum, 1 × antibiotics/antimycotics.

Human blood samples

The collection of human whole blood was approved by TSRI normal blood donor service. Fresh whole blood from TSRI normal blood donor service was drawn and kept at ambient temperature (in heparin-coated containers), followed by osmotic fragility test and P. falciparum infection experiments (see below) on the same day. Whole blood from Biological Specialty Corporation was delivered by air at ambient temperature the next day after collection for further experiments.

METHOD DETAILS

P. berghei infections and parasitemia measurement by flow cytometry

Donor mice (C57BL/6) were intraperitoneally injected with 50-200 μL of erythrocytes parasitized with either *P. berghei* (ANKA) GFPcon 259cl2 (provided by California Institute for Biomedical Research, La Jolla, USA) or *P. berghei* (ANKA) mCherry-hsp70-Luc-eef1a (line 1868 from Leiden Malaria Research Group, the Netherlands). We used *P. berghei* (ANKA) mCherry-hsp70-Luc-eef1a when infecting blood cell-specific *GOF Piezo1* mice because one of the Cre driver (EpoR-cre) has EGFP expression in RBCs so that *P. berghei* (ANKA) GFPcon 259cl2 cannot be used. Blood was collected by cardiac puncture from infected donors when the parasitemia reached 4%–6% (see below). Parasitized erythrocytes were washed with sterile saline three times at 1000xg for 3min and diluted to $5x10^5$ infected cells/ml as working solution. 200 μL working solution was intravenously injected into the experimental mice for analysis. For GFP-fluorescence based parasitemia measurement, 1.5 μL tail blood was collected from infected mice in 180 μL Dulbecco's Phosphate Buffer Solution with 2% fetal bovine serum, on 96-well plates. The cytometry

was performed on NovoCyte Flow Cytometer system (ACEA Biosciences, San Diego, CA) following manufacturer's instructions. Briefly, erythrocytes were selected on size for analysis by gating on forward/side-light scatter. Excitation of erythrocytes was performed with a laser at a wavelength of 488 nm and emission of the green fluorescence, or a wavelength of 587nm and emission of the mCherry was detected using a filter of 530 nm. By gating the uninfected erythrocytes and the GFP-positive infected erythrocytes parasitemia was calculated as the percentage of infected cells.

Blood-brain barrier and experimental cerebral malaria assay

When *P. berghei* infected displayed either experimental cerebral malaria (including ataxia, convulsion, paralysis and/or coma) or severe anemia (immobility and pale blood color), 2% Evans Blue (Sigma-Aldrich, dissolved in sterile saline) was intravenously injected into *P. berghei* infected at 5ml/kg body weight. After 45-60 min, euthanized mice were transcardially perfused with Phosphate Buffer Solution and 4% paraformaldehyde before brains were dissected. To quantify the Evan blue (EB) contents, the infected brains (n = 5 animals per genotype) were cut into small pieces and incubated in 1ml formamide at room temperature for 36 hours, followed by measuring the optical density at 620nm by Cytation3 (BioTek, Winooski, VT). The concentration of EB dyes was calculated from a standard curve with the equation (Y = 0.03263*X + 0.03413, where Y = reading, X = EB concentration). To quantify the brain water content, the infected mice (n = 5 animals per genotype) were sacrificed and brains were dissected. Brain tissues were weighted (wet weight), then dehydrated at 56°C. The sample was re-weighted 48hr later to obtain a dry weight. The percentage of water was calculated by: BWC = [(wet weight – dry weight) / wet weight] x 100%. Note there are cases that single brains were cut into half, with each half was used for both Evans blue and water content calculations.

Scanning Electron Microscope

Samples of mouse blood were added to ice cold buffered saline (10mM NaCl, 155mM KCl, 10mM glucose and 1 mM magnesium chloride) before being fixed in 2.5% glutaraldehyde in 0.1 M cacodylate buffer on ice. Aliquots of the fixed cells were placed on 12mm coverslips previously coated in polylysine for 30 mins. Following a buffer wash and postfixation in buffered 1% osmium tetroxide, the samples were extensively washed in distilled water. The samples were dehydrated in graded ethanol series followed by processing in a critical point drier (Tousimis autosamdri 815). The coverslips were then mounted onto SEM stubs with carbon tape and sputter coated with Iridium (EMS model 150T S) for subsequent examination and documentation on a Hitachi S-4800 SEM (Hitachi High Technologies America Inc., Pleasanton CA) at 5kV.

For human RBCs, samples were fixed at room temperature with 2.5% glutaraldehyde in 0.1M cacodylate buffer followed by 1% osmium tetroxide, and washed in water. A 10 μl drop of suspension was loaded on the sample carrier and imaged in a FEI Quanta200 FEG microscope in ESEM mode using the gaseous secondary electron detector. The stage was set-up at 2°C, the acceleration voltage was 15kV and the working distance 10 mm. Water was then progressively removed by cycles of decreasing pressure / injection of water, until reaching equilibrium at the dew point. The minimal final pressure in the chamber was 350 Pa. Pictures were taken with a dwell time of 6 μsec.

Osmotic fragility test and hematology test

Blood (for both mouse and human) was diluted at 1:8 into isotonic saline (0.9% NaCl) containing 2 mM HEPES, pH 7.4. 10 μL of the diluted blood was pipetted into each well (in a row) on a 96-well round-bottom plate. Separate rows were used for separate samples. 225 μL tonicity solutions made from saline solutions at concentration of 0, 20, 25, 30, 35, 40, 45, 50, 55, 60, 80, and 100%. The plate was incubated for 5min at room temperature followed by 5 min centrifuge at 1000xg. 150 μL supernatant was transferred to 96-well flat bottom plate for absorbance reading at 540nm using Cytation3 (BioTek, Winooski, VT). The data was analyzed using 4-parameter sigmoidal nonlinear regression. Hematological properties from mice were analyzed by hematology analyzer at Ruggeri lab, Department of Molecular and Experimental Medicine, The Scripps Research Institute, La Jolla, USA)

Gain-of-function Piezo1 mice generation

The targeting strategy was based on the NCBI transcript NM_001037298.1. Wild-type exons 45-51, including the complete 3' untranslated region (UTR) were flanked by loxP sites. An additional polyadenylation signal (nucleotide sequence of the synthetic polyA: gagctccctggcgaattcggtaccaataaaagagctttattttcatgatctgtgtgttggtttttgtgtgcggcgcg) was inserted between the 3′ UTR and the distal loxP site in order to prevent downstream transcription of the mutated exon 51 in the conditional allele. The size of the loxP-flanked region is 2.8 kb. The exons 45-51, including the splice acceptor site of intron 44 were duplicated and inserted downstream of the distal loxP site. The R2482H mutation was introduced into the duplicated exon 51. Positive selection markers were flanked by FRT (Neomycin resistance - NeoR) and F3 (Puromycin resistance- PuroR) sites and inserted into intron 44 and downstream of the synthetic polyA, respectively. The targeting vector was generated using BAC clones from the C57BL/6J RPCIB-731 BAC library and transfected into the TaconicArtemis C57BL/6N Tac ES cell line (Taconic, Hudson, NY). Homologous recombinant clones were isolated using double positive (NeoR and PuroR) selection. The conditional knock-in allele was obtained after Flp-mediated removal of the selection markers. The constitutive knock-in allele was obtained after Cre-mediated deletion of wild-type exons 45-51 and the synthetic polyA sequences

Mechanical stimulation

For whole-cell recordings, mechanical stimulation was achieved using a fire-polished glass pipette (tip diameter 3–4 μm) positioned at an angle of 80° to the recorded cells. Downward movement of the probe toward the cell was driven by a Clampex controlled piezoelectric crystal microstage (E625 LVPZT Controller/Amplifier; PhysikInstrumente). The probe had a velocity of 1 $\mu m.ms^{-1}$ during the ramp segment of the command for forward motion and the stimulus was applied for 150 ms. To assess the mechanical responses of a cell, the probe was first placed as close to the cell as possible (this distance could vary from cell to cell). Then, a series of mechanical steps in 1 μm increments was applied every 10 s, which allowed full recovery of mechanically activated (MA) currents. Threshold was calculated by subtracting the distance at which the probe first touched the cell surface from the minimal distance at which mechanically activated currents were evoked. Mechanically activated inward currents were recorded at a holding potential of −80 mV. The inactivation kinetics at a holding potential of −80 mV of traces of currents reaching at least 75% of the maximal amplitude of current elicited per cell were fitted with mono-exponential equation (or in some case bi-exponential equation for the rapidly-adapting currents, accordingly to previous reports (Albuisson et al., 2013) and using the fast time constant giving a value of inactivation time (τ) per responsive cell used for analysis. Channel kinetic properties between WT and mutant PIEZO1 were compared using Student's t test.

Cell culture and transient transfection

*PIEZO1*KO HEK cells were grown in Dulbecco's modified Eagle's medium containing 4.5 mg/ml glucose, 10% fetal bovine serum, 1 × antibiotics/antimycotics. Cells were plated in 6-well plates and transfected using lipofectamines 2000 (Invitrogen by ThermoFisher Scientific, Carlsbad, CA), according to the manufacturer's instruction. Human *PIEZO1* or mouse Piezo1 mutations fused to IRES-tdTomato was transfected at 1.4 μg per well (6-well plate) for fluorescent imaging plate reader (see below). To measure calcium signals, ultrasensitive sensor GCaMP6 (Chen et al., 2013) were transfected at 0.6 μg per well (6-well plate). Cells were incubated for 2 days before electrophysiology experiments or fluorescent imaging plate reader.

Fluorescent imaging plate reader (384-well format)

After transfection, the cells were dissociated from 6-well plates and re-seeded into 384-well plate, at 12,000 cells per well. The plate was incubated for 2 days then washed with assay buffer (1 × HBSS, 10 mM HEPES, pH7.4) using a ELx405 CW plate washer (BioTek, Winooski, VT). Fluorescence was monitored on a fluorescent imaging plate reader (FLIPR) Tetra. A 10-mM stock solution of Yoda1 in dimethyl sulfoxide (DMSO) was used resulting in a maximum of 1% DMSO in the assay. 10 μM Yoda1 was used in initial screens for searching gain-of-function mutations (compared to wild-type). Positive hits were then validated by using a series of Yoda1 concentrations. Concentration-response curves were fitted using a sigmoidal dose–response at variable slope (GraphPad Prism, La Jolla, CA).

Real time quantitative PCR.

Total RNA was isolated from mouse whole blood by Quick-RNA Whole Blood (Zymo Research, Irvine, CA). 500 ng total RNA was used to generate 1st strand cDNA using the Quantitect reverse

transcription kit (QIAGEN). Real time PCR assays were set up using GoTaq qPCR Master Mix (Promega, Madison WI). The reaction was run in the ABI 7900HT fast real time system using 1 μl of the cDNA in a 20 μl reaction according to the manufacturer's instructions in triplicates. Primers were designed for target gene (m*Piezo1*) and reference gene (*Gapdh*). See Key Resources Table for primer information. Calibrations and normalizations were done using the 2-ΔΔCT method, where ΔΔCT = ((CT(target gene) -CT (reference gene)) - (CT (calibrator) - CT (reference gene)).

CD4+ and CD8+ T cell isolation

MoJoSort Mouse CD4 and CD8 Nanobeads kits (BioLegend, San Diego, CA) were used for magnet-based cell separation of CD4/8+ T cells. We performed the procedures based on instructions provided by the kit manual.

Population genetic analysis

We obtained minor allele and genotype frequencies from the Exome Aggregation Consortium (ExAC) and the 1000 Genomes Project. 2504 genomes were analyzed, 661 from African and 1843 from non-African ancestries. Wright's fixation index (F_{ST}), a measure of population differentiation, was calculated as follows:

$$F_{ST} = \frac{\sigma_s^2}{\overline{p}\,(1-\overline{p})}$$

where $\overline{p}$ is the mean allele frequency and σ_s^2 is the allele frequency variance between the populations. The 1000 Genomes browser (http://phase3browser.1000genomes.org/index.html) was used to determine that no alleles were in linkage disequilibrium with E756del (estimated r^2 values were < 0.05). Hardy-Weinberg equilibrium was estimated using the classical binomial expansion to determine the expected genotype frequencies and x^2 tests.

PIEZO1 sequences were obtained from the following sources: modern humans (*Homo sapiens*, GenBank NG_042229.1), Neanderthals (*Homo neanderthalensis*, Neanderthal Ensembl ENSG00000103335), and Denisovans (*Homo sapiens* ssp. *Denisova*, previously generated reads (Meyer et al., 2012; Reich et al., 2010) aligning to humans [GRCh37/hg19] using the UCSC Genome Browser, (Kent et al., 2002)). All non-human primate amino acid sequences were obtained from GenBank. The sequences were aligned in Geneious using MAFFT (Katoh et al., 2002).

Genotyping in African American blood donors

Genotyping E756del carriers by sequencing

25 whole blood samples (5-10ml) were collected from Normal Blood Donor Service (The Scripps Research Institute, La Jolla, CA) and Biological Specialty Corporation (Colmar, PA), approved by institutional regulations. 200ul of whole blood samples were used for genomic DNA isolation by QIAamp DNA Blood Mini Kit (QIAGEN, Germany). A ~200bp PCR amplicon that contained E756 locus was generated for sequencing E756del or wild-type allele (forward primer: 5′CAGGCAGGATGCAGTGAGTG3′, reverse primer: 5′GGACATGGCACAGCAGACTG3′. Reverse primer was used for sequencing).

Screening for hemoglobin mutations by sequencing

PCR amplicons that contained potential sickle cell mutation sites were generated (Figure S5). Forward primers: 5′AGAA GAGCCAAGGACAGGTA3′; reverse primers: 5′TTGCAGCCTCACCTTCTTTC3′. Reverse primer was used for sequencing.

Screening for α-thalassemia by multiplex PCR

Each 50 μL reaction contained 20 mmol/L Tris-HCl pH 8.4, 50 mmol/L KCl, 1.5 mmol/L MgCl2, 1 mol/L betaine (SIGMA, St. Louis, MO), 0.2 μL of each primer (see below) 0.2 mmol/L of each dNTP, 2.5 units of polymerase, and 50-100 ng of genomic DNA. Reactions were carried out on a thermal cycler, with an initial 5-minute denaturation at 95°C, 30 cycles of 97°C for 45 s, 60°C for 1 minute 15 s, 72°C for 2 minutes 30 s, and a final extension at 72°C for 5 minutes.

Primers:

a2/3.7-F CCCCTCGCCAAGTCCACCC, 3.7/20.5-R AAAGCACTCTAGGGTCCAGCG, a2-R AGACCAGGAAGGGCCGGTG, 4.2-F GGTTTACCCATGTGGTGCCTC, 4.2-R CCCGTTGGATCTTCTCATTTCCC, SEA-F CGATCTGGGCTCTGTGTTCTC, SEA-R AGCCC ACGTTGTGTTCATGGC, FIL-F TGCAAATATGTTTCTCTCATTCTGTG, FIL-R ATAACCTTTATCTGCCACATGTAGC, 20.5-F GCCC AACATCCGGAGTACATG, MED-F TACCCTTTGCAAGCACACGTAC, and MED-R TCAATCTCCGACAGCTCCGAC

P. falciparum culture

P. falciparum Dd2 strain parasites were cultured under standard conditions (Trager and Jensen, 1976), using RPMI media supplemented with 0.05 mg/ml gentamycin, 0.014 mg/ml hypoxanthine (prepared fresh), 38.4 mM HEPES, 0.2% Sodium Bicarbonate, 3.4 mM Sodium Hydroxide, 0.05% O+ Human Serum (Denatured at 56°C for 40 min; Interstate Blood Bank, Memphis, TN) and 0.0025% Albumax). Human O+ whole blood was obtained from TSRI Normal blood donor service (La Jolla, CA). Leukocyte-free erythrocytes are stored at 50% hematocrit in RPMI-1640 screening media (as above, but without O+ human serum and with 2x albumax concentration) at 4°C for one to three weeks before experimental use. Cultures were monitored every one to two days via Giemsa-stained thin smears.

Parasitemia Determination

Asynchronous *P. falciparum* parasites (Dd2 strain) were cultured in standard conditions (as described above), then synchronized twice via sorbitol (Lambros and Vanderberg, 1979) and grown to 7% parasitemia at the late trophozoite/schizont stage. Patient blood was obtained from TSRI Normal blood donor service, washed and centrifuged three times (at 800 x g for 5 min at 4°C) with RPMI only and once with complete media (as above) (Elias and Greene, 1979), with any visible buffy coat being removed after each spin. All blood samples were given a numerical designation and allele status was not determined until after all data collection was completed. All genotypes were blinded from experimenters. (Basic Malaria Microscopy, 2010)

Parasite growth was determined in two independent ways: absolute parasitemia determination via thin-blood smear after Giemsa staining, and inferred parasite growth via the SYBR Green I-based fluorescence assay (Johnson et al., 2007). For the absolute parasitemia determination by thin blood smear, parasites were established, starting from the 7% parasitemia cultures above and diluted using the corresponding patient RBCs, in a 10 mL culture at 5% hematocrit and 0.5% parasitemia (the same as for the Giemsa absolute parasitemia determination assay). Cultures were then grown for 4 days and parasitemia measurements were taken every 2 days. For the SYBR green I inferred parasitemia determination assay, when parasite burden is estimated based upon DNA content, parasites were cultured in 100 μL volumes in 96-well plates at 5% hematocrit and 0.5% parasitemia with at least 5 replicates per time point. Parasites were plated on three 96-well black plates with clear bottoms (Fisher Scientific). (One surrogate plate was used for measurement every two days, with DNA content determined by SYBR Green I incorporation of lysed parasites). Relative parasitemia was determined by fluorescence measurement, background was determined using uninfected RBCs and subtracted, then relative parasite burden was determined via normalization against a known O+ WT blood sample. In both cases all measurements were taken for all samples, genotypes were then assigned to numbered patient samples, wild-type versus heterozygote samples were averaged at each time point, and average parasitemia values were compared.

QUANTIFICATION AND STATISTICAL ANALYSIS

Statistical analysis

All of the data are presented as the mean ± SEM or SD and represent at least 3 independent experiments. Statistical analysis, significance level and n values are described in the Figure or Figure legends. For mouse experiments n = number of animals and at least n = 4 were used. For human blood experiment, n = number of individual blood samples. For comparison, we performed two-tailed Student's t test, where $p < 0.05$ is considered statistically significant. For all datasets, we used Prism7 to perform the statistical analysis.

Cell

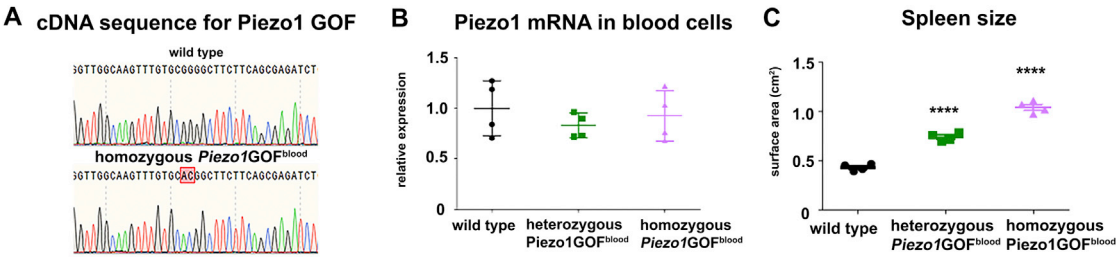

Figure S1. *Piezo1* GOF Mice Characterization, Related to Figure 1

(A) Modified nucleotides in the last exon of piezo1 cDNA from homozygous *Piezo1*GOF ^{blood} (lower). GG to AC change compared to wild-type (upper).

(B) *Piezo1* transcript levels in *Piezo1*GOF ^{blood} mice, $p > 0.05$ (One-way ANOVA test).

(C) Spleens from *Piezo1*GOF ^{blood} mice are significantly larger than wild-type. ****$p < 0.0001$, Student's t test, both compared to wild-type (n = 3 for each group).

Data are presented as means ± SEM.

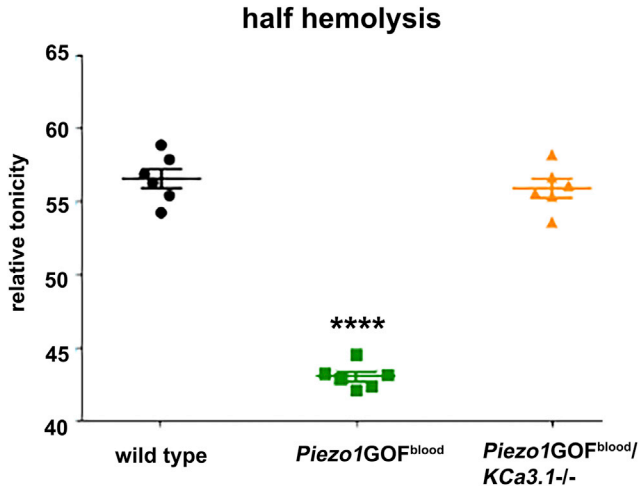

Figure S2. *Piezo1*GOF ^{blood}/*KCa3.1*$^{-/-}$ Mice RBC Phenotype, Related to Figure 3

*Piezo1*GOF ^{blood}/ *KCa3.1*$^{-/-}$ mice had normal RBC osmotic fragility as wild-type ($p > 0.05$), which are significantly larger than heterozygous *Piezo1*GOF ^{blood} mice (****$p < 0.0001$). Data are presented as means ± SEM.

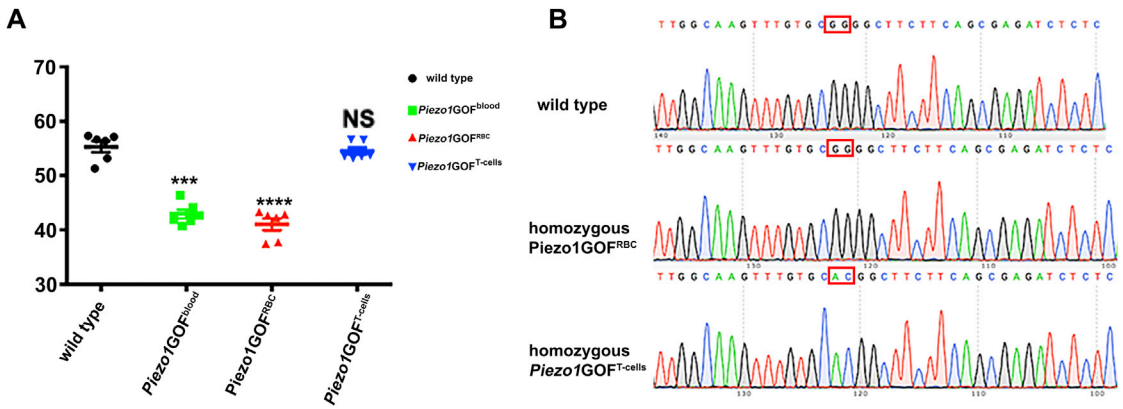

Figure S3. *Piezo1*GOF ^{RBC} and *Piezo1*GOF $^{T\ cells}$ Mice Characterization, Related to Figure 4

(A) *Piezo1*GOF ^{RBC} mice had RBC dehydration, similar to *Piezo1*GOF ^{blood} (***$p < 0.001$ and ****$p < 0.0001$ compared to wild-type, Student t test), while *Piezo1*GOF $^{T\ cells}$ had normal RBC osmotic fragility ($p > 0.05$ compared to wild-type, Student t test).

(B) cDNA showed that CD4+ and CD8+ T cells expressed *Piezo1* mRNA with gain-of-function mutation (AC in red square) in homozygous *Piezo1*GOF $^{T\ cells}$ mice (lower panel), whereas wild-type and homozygous *Piezo1*GOF ^{RBC} mice expressed wild-type (GG in red square) mRNA (upper and middle panels). Data are presented as means ± SEM.

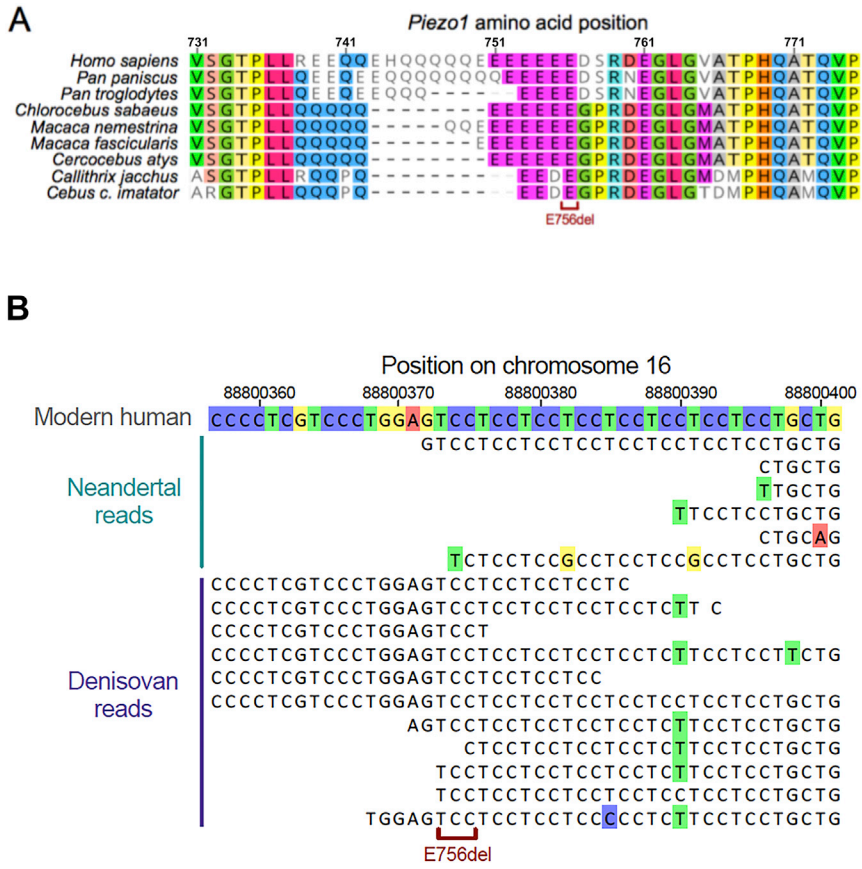

Figure S4. Comparative Genomics, Related to Figure 6

E756del locus in non-human primates, pre-modern humans, and modern humans.

(A) An amino acid alignment of human and non-human primate PIEZO1 sequences (partial). Highlighted amino acids indicate consensus among all sequences and dashes indicate gaps.

(B) Sequences of individual Neanderthal and Denisovan reads (see STAR Methods) were aligned to human chromosome 16. Shown is the region near the E756del locus in PIEZO1.

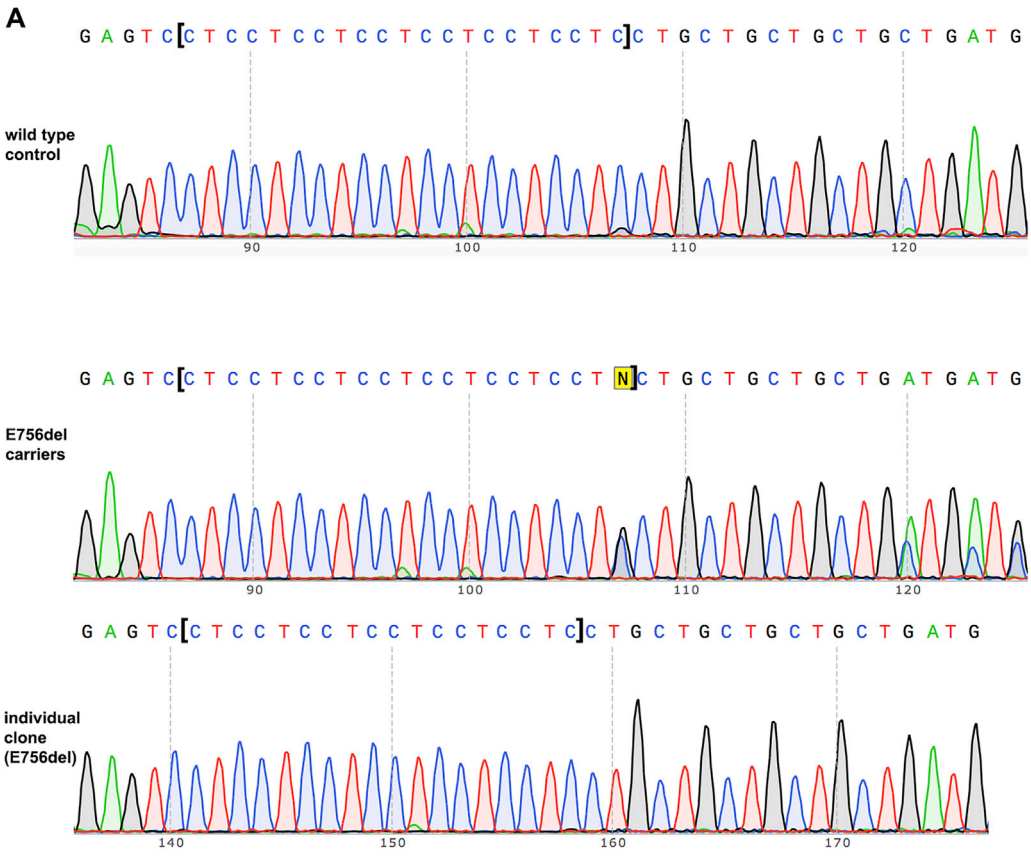

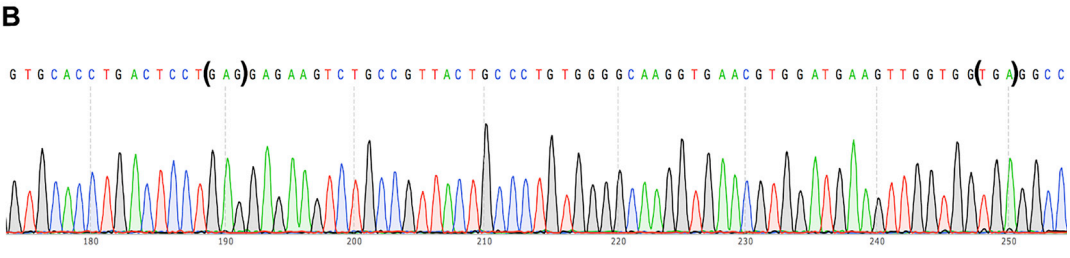

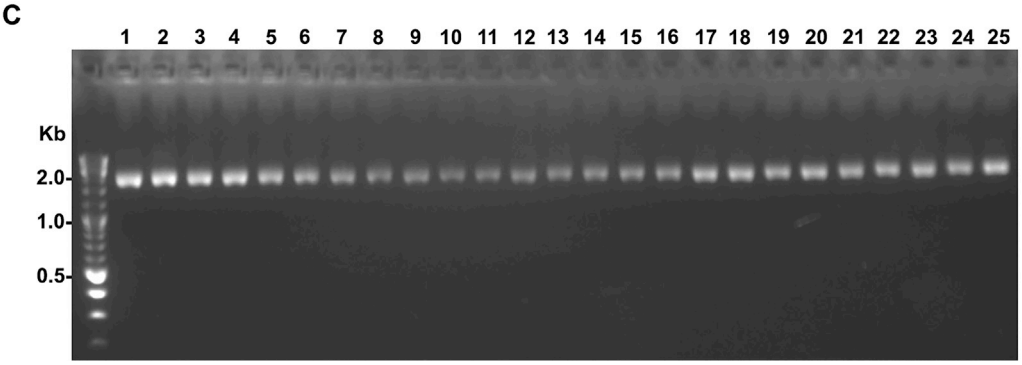

(legend on next page)

Figure S5. Genotypes of African American Blood Donors, Related to Figure 7

(A) Screening for E756del in 25 donors. Upper panel: sequence of a ~200bp PCR amplicon that contains E756 locus in control donors showed 7 repeats of CTC (in squared brackets). Middle panel: E756del heterozygous carriers showed an ambiguous base at the 7th CTC repeat (in squared brackets). Lower panel: individually cloned PCR amplicon from carriers showed the presence of E756del.

(B) Hbb (β-globin) gene from 25 donors showed normal sequence, excluding HbC, HbS (first brackets) and HbE (second brackets).

(C) All 25 donors had normal PCR production (~1.9kb band) for α-globin gene in a multiplex PCR screening protocol.